F. Fusi, A. Guardone, G. Quaranta, P.M. Congedo
Multifidelity Physics-Based Method for Robust Optimization Applied to a Hovering Rotor Airfoil
AIAA Journal, Vol. 53, N. 11, 2015, p. 3448-3465
doi:10.2514/1.J053952

Multi-fidelity physics-based method for robust optimization with application to a hovering rotor airfoil

Francesca Fusi*, Alberto Guardone† and Giuseppe Quaranta‡

Politecnico di Milano, Milano 20156, Italy

Pietro M. Congedo§

INRIA Bordeaux Sud-Ouest, Talence Cedex 33405, France

The paper presents a multi-fidelity robust optimization technique with application to the design of rotor blade airfoils in hover. A genetic algorithm is coupled with a non-intrusive uncertainty propagation technique based on Polynomial Chaos expansion to determine the robust optimal airfoils that maximize the mean value of the aerodynamic efficiency while minimizing the variance, under uncertain operating conditions. Uncertainties on the blade pitch angle and induced velocity are considered. To deal with the variable operating conditions induced by the considered uncertainties and to alleviate the computational cost of the optimization procedure, a multi-fidelity strategy is developed which exploits two aerodynamic models of different fidelity. The two models corresponds to different physical descriptions of the flowfield around the airfoil; thus, the multi-fidelity method employs the low-fidelity model in regions of the stochastic space where the physics of the problem is well-captured by the model, and switches to high-fidelity estimates only where needed. The proposed robust optimization technique is compared with the robust optimization based on the high-fidelity aerodynamic model and the deterministic optimization, to assess the capability of finding a consistent Pareto set, and to evaluate the numerical efficiency. The results obtained show how the robust multi-fidelity

*Phd student, Dept. Aerospace Science and Technology, Via La Masa 34, 20156 Milano, Italy.
†Associate professor, Dept. Aerospace Science and Technology, Via La Masa 34, 20156 Milano, Italy.
‡Assistant professor, Dept. Aerospace Science and Technology, Via La Masa 34, 20156 Milano, Italy.
§Research Scientist, Team BACCHUS, 200 Rue de la Vieille Tour, Talence Cedex 33405, France.

approach is effective in reducing the sensitivity of the designed airfoils with respect to variation in the operating conditions.

Nomenclature

A_i^c, A_i^t	=	Bernstein polynomial coefficients for camber and thickness distribution
C	=	class function
C_{D_W}	=	wave drag coefficient
C_f, C_p	=	friction and pressure coefficients
E	=	lift-to-drag ratio or efficiency
$\mathbf{g}$	=	optimization constraints
$\mathcal{L}$	=	aerodynamic model operator
M	=	Mach number
n	=	Bernstein polynomial order
N	=	number of terms of polynomial chaos expansion
n_o	=	polynomial order of polynomial chaos expansion
n_p	=	number of points on airfoil surface
n_s	=	number of samples in stochastic space
$n_{\boldsymbol{\xi}}$	=	number of uncertain variables
p	=	probability density function
p_α	=	probability density function of angle of attack
p_θ, p_{V_i}	=	probability density function of blade pitch angle and induced velocity
$p_{\boldsymbol{\xi}}$	=	probability density function of uncertain variables
$\mathbf{q}$	=	flowfield unknown variables vector
r	=	percentage of blade radius
Re	=	Reynolds number
S	=	shape function
u, v	=	output stochastic variables
V_i	=	induced velocity [m/s]
$\mathbf{x}$	=	space variables
$\mathbf{y}$	=	design variables
α	=	angle of attack [deg]
α_k	=	polynomial chaos coefficient
ϕ_i	=	univariate polynomial of polynomial chaos expansion

μ	=	mean value
ψ	=	adimensional chordwise coordinate
Ψ_k	=	multivariate polynomial of polynomial chaos expansion
σ^2	=	variance
Σ	=	design space
τ	=	threshold of multi-fidelity method
θ	=	blade pitch angle [deg]
$\boldsymbol{\xi}$	=	input stochastic variables
Ξ	=	stochastic space
ζ	=	adimensional airfoil coordinate
$\tilde{\zeta}, \zeta_{CST}$	=	adimensional exact and obtained by parameterization airfoil coordinate
ζ_c, ζ_t	=	adimensional coordinate of camber and thickness distributions
$\zeta_u \zeta_l$	=	adimensional coordinate of upper and lower surfaces

I. Introduction

A powerful tool for aerodynamic design is shape optimization, that is the process of finding the shape that provides the best performance given a set of objectives and constraints. Shape optimization has played a key role in aerodynamic design since its very beginning: initially, the optimization was performed with analytical tools whenever possible and with a "trial and error" approach based on the wind tunnel testing of preferred design solutions. Modern shape optimization relies on the coupling of numerical optimization methods and Computational Fluid Dynamics (CFD) solvers;[1] this combination was first experimented in the 70s with the work of Hicks and Henne[2] and was widely developed in the 90s[3,4] thanks to the great potential provided by CFD tools. The application of optimization to wing aerodynamic design has proved effective in indicating directions of improvement of a current design with gradient-based methods,[5] or exploring the design space by means of global optimizers, such as evolutionary algorithms.[6] Although airfoil optimization is well-established in the scientific literature, a concerted effort is still needed to exhaustively tackle the case of helicopter rotor blades. In fact, rotor blades feature complex aerodynamics with unsteady effects due to the blade dynamics and the interaction with vortices and wakes trailed from preceding blades. As a result, the complexity of the flowfield and the largely variable flow conditions encountered by rotor blades have limited the development of comprehensive aerodynamic optimization algorithms.[7] Few interesting examples of rotor aerodynamic optimization can be found in Refs.,[8–12] where the optimization is more focused on blade twist and planform

parameters.

A. Background on robust design

In the past decade, great attention has also been drawn to uncertainty-based optimization, that is the process of finding the optimal design of a particular engineering system when taking into account the uncertainty affecting the system itself in terms of model, parameters, or design variables. As a matter of fact, engineers generally employ design and optimization methods considering all relevant aspects of the system operating cycle, in which inherently exist numerous sources of uncertainty. For instance, a theoretical model of the actual system is based on assumptions and simplifications that introduce errors in the prediction of the performance. In addition, a large portion of the data necessary to build the numerical model is affected by numerous sources of uncertainty. Suffice it to say, system operating conditions are affected by the status of the surrounding environment. In other words, some model parameters used to represent the physical system are affected by a lack of knowledge of the system itself. These uncertainties may alter the system's expected performance, jeopardize the safety, and even result in mission failure. In order to take uncertainties into account from the beginning of the design, the research community focused on uncertainty-based optimization techniques, such as robust optimization methods which seek an optimal design that is capable of satisfactory performance when considering the variability of system parameters.[13,14]

Robust design can be intrinsically more fit than classical deterministic approaches for very preliminary design phases, since its objective can be interpreted as the search for optimal solutions that have a low sensitivity to variations of the parameters in the range of uncertainty. In turn this may reduce the probability of redesign at later stage of the design process due to lack of adequate performance. Robust approaches have been studied in the field of aerospace vehicles with application to conceptual, structural and aerodynamic design.[15]

Uncertainty types. With regard to aerodynamic design, some works consider the so-called aleatory uncertainties, namely irreducible uncertainties arising from the inherent variation associated with the system.[16] For instance, uncertainties on the geometric parameters[17–19] and on the operating conditions[20,21] fall into this category. Other research focused more on epistemic uncertainties, which represent a lack of knowledge associated with the modeling process that are reducible through the introduction of additional information.[22] Some works, like the one presented in Ref.,[23] combine aleatory uncertainty on the freestream Mach number with an epistemic uncertain variable, i.e. the kinematic eddy viscosity of the the Spalart-Allmaras model.[24]

ROBUST OPTIMIZATION METHODS. Once the sources of uncertainty and the corresponding uncertain variables are identified, a robust optimization procedure can be set up. The robust optimization loop is typically based on the coupling of an optimization algorithm and an uncertainty quantification method. The latter provides the statistical moments of a given quantity of interest starting from the system model. When a "non-intrusive" quantification method is employed,[25] many samples of the quantity of interest are required and those are obtained by means of a computational model of the system. In the case of an aerodynamic system, the computational model can be provided by an accurate, high-fidelity CFD tool, for example. However, in a robust optimization loop many CFD computations are required for each geometry or design, and this inevitably aggravates the cost of the optimization procedure.

To alleviate this cost, the numerical model of the aerodynamics provided by the accurate, yet expensive, CFD solvers could be replaced with a lower-fidelity model. Examples of this type of model are potential flow models, which have been employed in the past both in fixed wing[26] and rotor airfoil design,[27,28] as well as surrogate models of the performance, such as response surfaces.[29] These models may require a small amount of CPU time, but their range of applicability is limited and accuracy may be poor.

MULTI-FIDELITY METHODS. An alternative approach is based on the combined use of models of different fidelity and level of approximation in order to try to balance computational cost with the accuracy required. In the literature this solution is usually referred to as multi-fidelity optimization and it has been already applied in deterministic optimization.[30–32] In the last years, some applications have considered the problem of uncertainty-based airfoil optimization, as well. Among these, a multi-fidelity method is developed in Refs.[33,34] based on a hierarchical kriging approximation which exploits an estimate of the solution obtained by the same CFD solver, applied to fine grids for obtaining high fidelity results, and to coarser meshes for low fidelity ones. Another approach presented in Ref.[35] is based on the application of the uncertainty quantification technique to the system response obtained by the low-fidelity model and to the correction function, i.e. the discrepancy between the high-fidelity model and the low-fidelity model. In this work the multi-fidelity is built with respect to the the different degree of accuracy of the physical models used to describe the flowfield.

A multi-fidelity robust stategy is here proposed for the optimization of airfoils to be employed on helicopter rotor blades. The motivation is twofold. First, due to the complex aerodynamics associated with helicopter rotors, even when considering a single flight condition, blade airfoils are required to operate under variable flow conditions, due to many factors, including interactions with fuselage and tail rotor, tip vortices, wakes trailed from preceding blade (see Fig. 1). This could result in the necessity to consider a wider range of

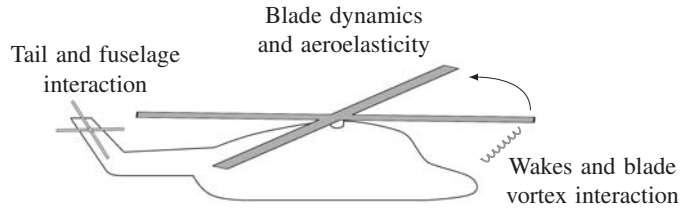

Figure 1. Characteristics of the complex flowfield around a helicopter rotor in hover.

operating angle of attack, Mach number and Reynolds number with respect to fixed-wing applications. Indeed, this complex aerodynamic flowfield requires an accurate prediction which can be achieved by means of high fidelity CFD tools based on Reynolds Average Navier Stokes (RANS) equations. Unfortunately, these CFD solvers can be very expensive from a computational point of view, especially when employed in the design stage where a large number of solutions is needed. This leads to the second motivation: when performing an optimization under uncertainties, multi-fidelity strategies represent a viable solution to the huge demand of computational resources required for rotorcraft applications.

B. Objectives of the paper

The present work focuses on the development of a multi-fidelity strategy for the optimal design of rotor airfoils under uncertain operating conditions. To avoid an unnecessary increase of complexity of the presentation of the optimization strategy it has been chosen to limit the application to one particular design condition: the hover. The basic elements of the robust optimization method are the Non-dominated Sorting Genetic Algorithm for the optimization loop, and the Polynomial Chaos (PC) expansion for the non-intrusive uncertainty propagation. The PC method reconstructs the objective functions starting from samples computed by the chosen aerodynamic model. The multi-fidelity strategy is exploited to limit the computational cost associated with the uncertainty propagation through the aerodynamic models.

In particular, two aerodynamic models are considered in the multi-fidelity strategy: (i) a compressible coupled Euler equations/integral boundary layer solver and (ii) an aerodynamic solver coupling a panel method and integral boundary layer model. The former is more expensive than the latter from a computational point of view. However, it is more accurate in those operating conditions that exhibit important compressible effects. The proposed multi-fidelity method switches from the low-fidelity model to the high-fidelity model only in those operating conditions. Unlike most multi-fidelity methods in aerodynamic optimization,

the switching logic here is based on physical considerations, so the multi-fidelity approach can be labeled as physics-based. The low-fidelity physical model does not require training and training data at each optimization loop, as surrogate models do. An example of a similar approach in the literature for deterministic aerodynamic optimization is presented in Ref.[36]

The paper is organized as follows. In Section II the optimization problem is formulated for this specific case. Section III describes the ingredients of the method employed to perform the robust optimization: the uncertain operating conditions, the aerodynamic models, the shape parameterization, the optimization algorithm and the uncertainty quantification technique. In Section IV the proposed multi-fidelity strategy is presented, with some preliminary results of the strategy obtained for a reference airfoil. Finally, Section V shows the results of the robust optimization algorithm coupled with the low- and high-fidelity models, and those of the proposed multi-fidelity strategy.

II. Robust optimization problem

The robust optimization technique proposed in this paper is applied to the optimal selection of the airfoil for a helicopter rotor blade in hover. Ideally the hover condition is a perfectly simmetric and steady flow condition when an isolated rotor is considered. However, when a rotor is installed on the helicopter (see Fig. 1) the interference with the other parts and the necessity to trim the entire aircraft requires the introduction of some cyclic pitch commands that lead to variable flow conditions met by the blade section in different azimuth position. As a consequence, instead of considering a deterministic, representative operating condition for hover, it is assumed that the freestream condition of the airfoil section is affected by some level of uncertainty. In this paper we deal with sources of uncertainty in the physical modelling employed at the design stage. This uncertainty could arise from errors in the model representation (e.g. the blade inflow model). Additionally, other physical sources of uncertainty may be considered, such as those related to blade structural flexibility, that may modify the local pitch angle. Because in the design stage the blade pitch angle θ and the induced velocity V_i dictate the operating condition of the airfoil, uncertainties on these two system parameters are considered in the present analysis. The induced velocity is also a freestream boundary condition that permits consideration of the effect of the wake vorticity of the blade on the airfoil in a simple yet effective way.[37]

The objective of the aerodynamic optimization is to maximize the lift-to-drag ratio E, which is a measure of the aerodynamic efficiency of the airfoil. This measure is chosen because improving the lift-to-drag ratio in the airfoil selection benefits the rotor performance.[38] The objective of this analysis is mainly to find a robust optimal airfoil shape. When considering variable operating conditions, the term "robustness" has various meanings depending

on the desired objective.[20] It could indicate (i) a design that is minimally sensitive to a variability either in the system or in the design itself, (ii) a design that uniformly improves the performance of the system over a set of operating conditions, (iii) a design with an improved worst-case performance, and (iv) a design that improves the overall performance over the entire range of operating conditions and/or lifetime. In this paper, robustness means that the design parameters $\mathbf{y}$ defining the shape of the airfoil allows simultaneous improvement in the overall performance and minimization of the sensitivity with respect to changes in the system operative conditions. In other words, the optimal design must maximize the mean value μ_E and minimize the variance σ_E^2 of the objective function, computed by taking into account the uncertainties of the operating conditions. Unlike single-objective optimization where there is only one global optimum, in the case of multi-objective optimization, as the one under consideration here, there is a set of optimal solutions (the so-called Pareto front) corresponding to various trade-offs between the mean value and the variance.

The objective function E is a function of the output of the aerodynamic system, that is the solution of the differential equation modelling the aerodynamics:

$$\mathcal{L}\left(\mathbf{x}, \mathbf{y}, \boldsymbol{\xi}; \mathbf{q}(\mathbf{x}, \mathbf{y}, \boldsymbol{\xi})\right) = 0, \tag{1}$$

where $\mathcal{L}$ is a nonlinear spatial differential operator describing the problem. The solution of the stochastic equation (1) is the vector $\mathbf{q}(\mathbf{x}, \mathbf{y}, \boldsymbol{\xi})$, which contains the unknown variables, e.g. density, momentum and total energy. The solution vector $\mathbf{q}$ is a function of the two-dimensional space variable $\mathbf{x} \in \mathbb{R}^2$, the design variables $\mathbf{y}$ belonging to the design space Σ, and the uncertain input parameters $\boldsymbol{\xi}$ belonging to the stochastic space Ξ.

The differential equation (1) represents a constraint for the optimization problem. Additional constraints are related to manufacturing feasibility and costs. The geometry of the airfoil is constrained in such a way that only airfoils having at most one inflection point of the camber line are allowed, and the pitching moment coefficient computed at the quarter-chord location is constrained to prevent excessive torque on the blade structure. The latter constraint is applied when the moment coefficient about the quarter-chord location exceeds 0.03. Despite the importance of minimizing the pitching moment, such a value is chosen to explore the design space with sufficient freedom. Additional objectives, such as the minimization of the moment coefficient, could be included in future works, to define an even better optimal solution for helicopter rotor blades.

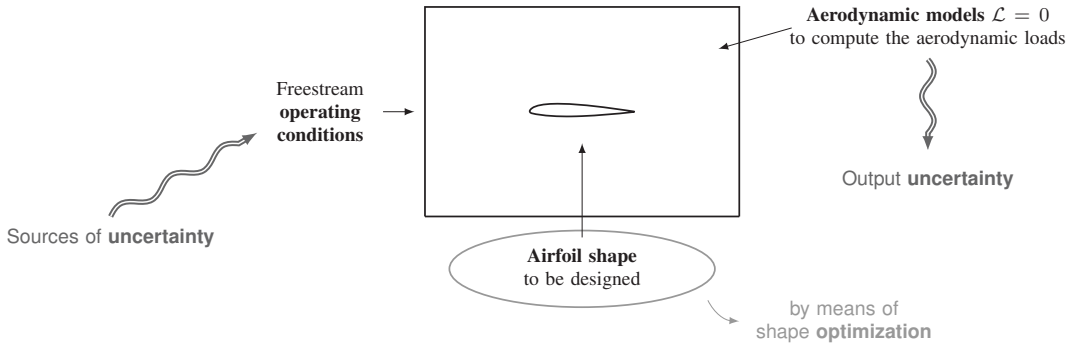

Figure 2. Representative scheme of the optimization problem of the airfoil shape under uncertainty.

In mathematical terms, the resulting optimization problem can be stated as:

$$\begin{aligned} \text{maximize:} \quad & \mu_E\left(\mathbf{q}\left(\mathbf{x},\mathbf{y},\boldsymbol{\xi}\right)\right) \\ \text{and minimize:} \quad & \sigma_E^2\left(\mathbf{q}\left(\mathbf{x},\mathbf{y},\boldsymbol{\xi}\right)\right) \\ \text{subject to:} \quad & \mathcal{L}\left(\mathbf{x},\mathbf{y},\boldsymbol{\xi};\mathbf{q}(\mathbf{x},\mathbf{y},\boldsymbol{\xi})\right) = 0 \\ & \mathbf{g}\left(\mathbf{x},\mathbf{y},\boldsymbol{\xi};\mathbf{q}(\mathbf{x},\mathbf{y},\boldsymbol{\xi})\right) \leq \mathbf{0} \\ \text{by changing:} \quad & \mathbf{y} \end{aligned} \tag{2}$$

with uncertain input parameters $\boldsymbol{\xi} = \{\theta, V_i\}$ and under the constraints previously described and collected in vector $\mathbf{g}$. The robust optimization problem requires several ingredients (Fig: 2): (i) a model of the aerodynamic system which includes the aerodynamic model ($\mathcal{L} = 0$) which describes the flowfield around the airfoil, the freestream boundary conditions and the airfoil shape, (ii) an uncertainty quantification method that propagates the uncertainty affecting the freestream operating conditions to the uncertainty on the output, i.e. the aerodynamic loads computed by means of the aerodynamic model , and (iii) a shape optimization method that seeks to find the best design according to the objectives and contraints set in Eq. (2).

III. Numerical ingredients of robust optimization method

In robust optimization two nested loops are implemented: the outer loop of the optimization algorithm, and the inner loop of the uncertainty propagation technique (see Fig. 3). In particular, at each k-th iteration of the outer optimization loop the stochastic analysis is performed in order to evaluate the statistical moments μ, σ^2 of the objective for the current design $\mathbf{y}_k$. The uncertainty quantification method is thus employed as a black box by the op-

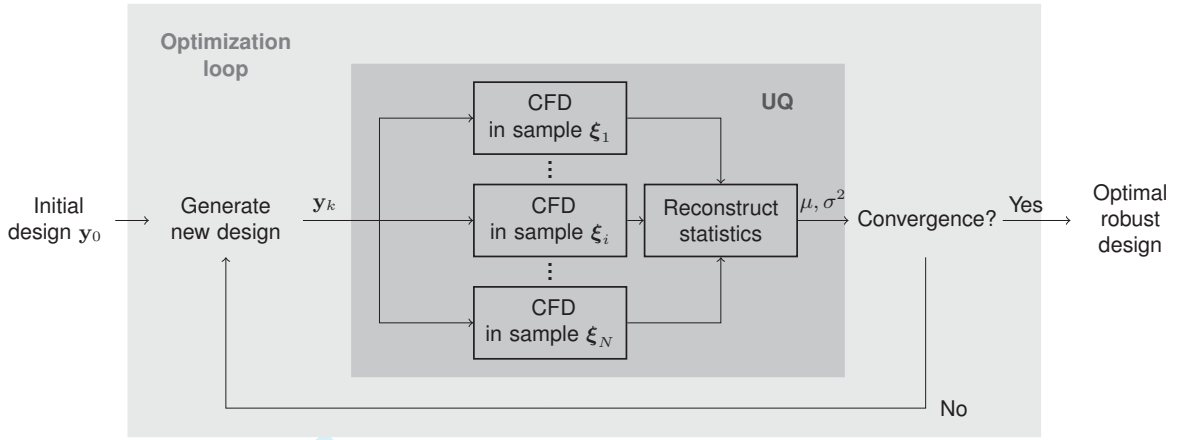

Figure 3. Block diagram of the uncertainty-based optimization loop.

timization algorithm. In the following, the numerical ingredients used in the implementation of the robust optimization problem are discussed.

A. Uncertain operating conditions

In this work, a reference, or nominal, condition is first chosen which represents a typical condition for a section of a blade in hover. Then, an estimate of the uncertainty on each variable is computed. For the nominal condition, data from Ref.[39] are employed, considering two blade sections respectively at 40% and 80% of the span (see Tab. 2). The blade pitch angle and induced velocity are computed by means of the Blade Element Momentum Theory (BEMT) starting from data of the Bo105 rotor and assuming a radial distribution of inflow on the blades [40, p. 127]. Regarding the uncertain parameters, a variation of ± 2 deg is estimated for the blade pitch angle due to longitudinal cyclic and lateral cyclic pitch, and a value of ± 0.5 deg is added in order to model the effect of blade flexibility with an uncertainty in the torsional stiffness. This level of uncertainty has also been found on the pitch measures taken during the HART II experimental campaign.[39] For the induced velocity, a variation of $\pm 10\%$ of the nominal value is considered due to the modeling of physical parameters of

Table 2. Nominal operating conditions.

r [-]	V_i [m/s]	θ [deg]	α [deg]	M [-]	Re [-]
0.4	10.52	10.11	6.0	0.258	1.6e6
0.8	13.82	9.71	5.2	0.513	3.2e6

Table 3. Uncertainty on blade pitch angle θ and induced velocity V_i.

Variable	Uncertainty	PDF type
V_i	$\pm$ 15%	Uniform
θ	$\pm$ 2.5 deg	Uniform

the system; such a level of uncertainty has been assessed in Ref.[41] as a result of uncertainty on both aerodynamic and structural uncertainties such as blade chord, air density, and rotor angular velocity. Furthermore, a $\pm$5% is added based on empirical considerations to approximate the effects of the losses due to the wakes trailed from the blades and other three-dimensional effects of the rotor which are not yet known in the design stage of the blade.

In addition, the uncertain variables $\boldsymbol{\xi} = \{\theta, V_i\}$ are modelled in a probabilistic framework, meaning a probability density function is assigned to each variable. In particular, a uniform probability density function is adopted (see Fig. 4(a)) in order to consider the worst-case scenario among the probabilistic descriptions. That is the one where each event in the uncertainty range is just as probable as the nominal condition (see Tab. 3). Another modelling assumption is that the uncertain variables are independent, which may not be true to some extent due to the connection between the rotor induced flow and the blade control. However, because the complete aero-servo-elastic system is not under examination but only the aerodynamic subsystem, the two variables are considered as separate and independent.

The uncertainties of the induced velocity V_i and the blade pitch angle θ affect the conditions of the flowfield around the airfoil. In particular, its influence on the airfoil angle of attack is the most significant, while minor effects are noticed on the Mach and Reynolds numbers. The level of uncertainty considered for each variable is consistent with those typically employed in the literature of uncertainty-based analysis in fluid dynamics (e.g. Refs.[42–44]). Their combined effect results in a large variation of the angle of attack once it is propagated through the BEMT equations. Such a variation is up to 60%, as shown in Fig. 4(b) for the section at 80% of the radius. The angle of attack has a fundamental role on the onset of boundary layer instability, the occurrence of large flow separation and the development of complex compressibility effects. In this case, taking uncertainty into account yields large variations of the flowfield characteristics, and the most significant effect is associated with compressibility. To show the above in a straightforward manner, the critical Mach number is computed at different angles of attack for the NACA 0012 airfoil by combining the isentropic one-dimensional flow equation for pressure with either the Prandtl-Glauert or the Karman-Tsien correction rule for the pressure coefficient [45, p. 325]. The result is plotted in Fig. 5(a), where the variablity range of the flowfield parameters, angle of attack and Mach

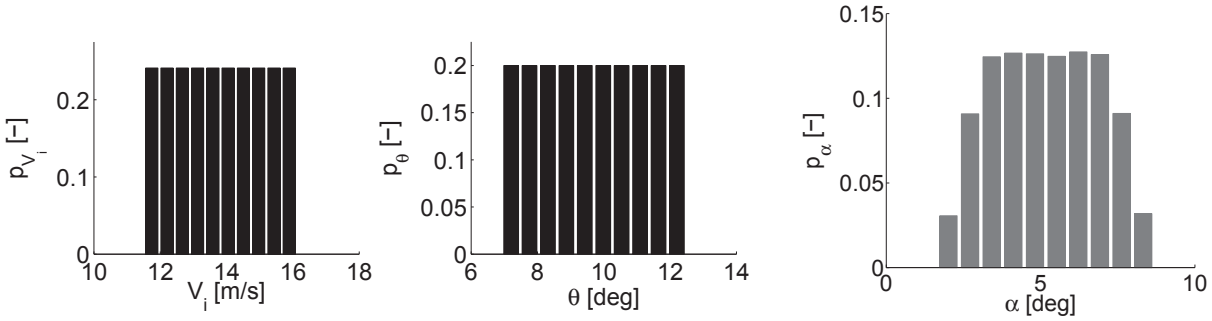

(a) Input uncertainty on induced velocity V_i and blade pitch angle θ

(b) Resulting uncertainty on the angle of attack α

Figure 4. Uncertainty on the operating conditions (section at $r = 0.8$).

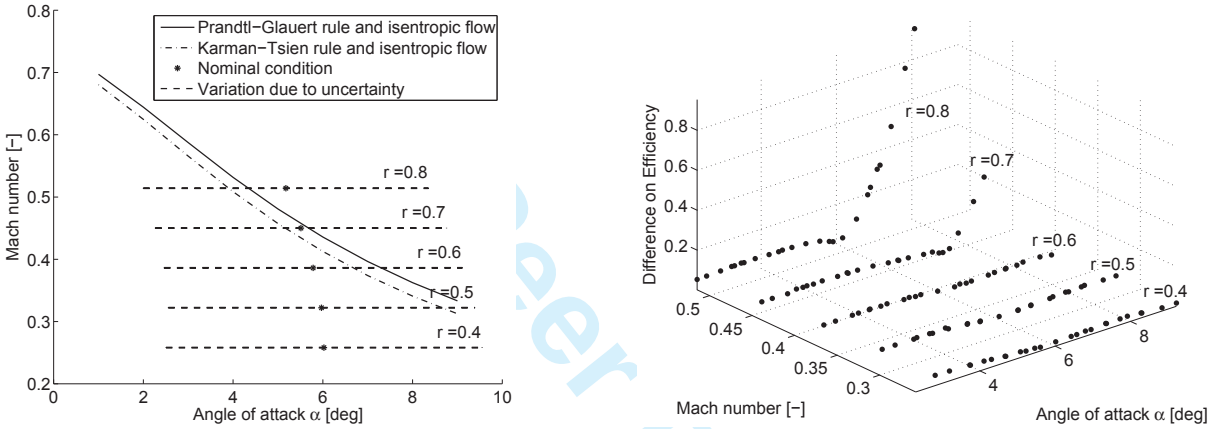

(a) Critical Mach number and uncertain operating conditions

(b) Relative difference in the estimates of the efficiency between high and low fidelity models

Figure 5. Analysis of the effect of uncertain operating conditions on the critical Mach number (a) and on the estimates of the airfoil efficiency (b) for the NACA 0012 airfoil.

number, is also presented for different blade sections. It appears that for sections located at a distance from the root greater than 60% of the radius, the variability range crosses the critical Mach curve, which represents the onset of significant compressibility effects.

B. Aerodynamic models

As presented in the preceding section, computations both in the subsonic and low transonic range are required to reconstruct the mean and the variance of the performance. In transonic conditions, only aerodynamic solvers dealing with nonlinear compressible effects yield meaningful estimates. However, the computational cost increases when using compressible aerodynamic models. Under the critical Mach curve, instead, cheaper computations can be performed with a subsonic, linear model. As a result, two aerodynamic models are considered, which corresponds to different level of fidelity: a low-fidelity model suited for flow past

an airfoil in subsonic flow, and a high-fidelity model for (low) transonic conditions.

1. *Low-fidelity model*

The low-fidelity solver is XFOIL, an aerodynamic solver which couples panel and integral boundary layer methods developed for the analysis of subsonic, isolated airfoils.[26] The outer flowfield is modelled with an inviscid linear vorticity panel-based method, which is coupled to the viscous layers represented by the two-equation lagged dissipation integral method in order to correct the potential flow with the viscous boundary layer. Here, the transition of the boundary layer is predicted by applying the e^n criterion, while compressible effects for low Mach numbers are taken into account by the Karman-Tsien correction. This model is well suited for the simulation of flows around an airfoil at moderate values of the angle of attack and Mach number, and it permits a rapid evaluation of the aerodynamic coefficients.

2. *High-fidelity model*

The high-fidelity solver is MSES,[46] a coupled Euler/integral boundary layer code for the analysis and design of multi-element or single-element airfoils. It couples the solution of the Euler equations implemented with a streamline-based discretization for the outer field with a two-equation integral boundary layer formulation for the thin region close to the airfoil. The coupling is performed by means of the displacement thickness and the system equations are solved simultaneously by a full Newton method. The prediction of the boundary layer transition from laminar to turbulent flow is carried out either with the full e^n method[47] or with the simplified envelope method.[48] Thus, the MSES solver is capable of representing the nonlinear compressibility effects arising in the transonic flow regime.

3. *Comparison of aerodynamic models*

Although the two models share a similar modelling of the boundary layer, the high-fidelity solver is capable of representing the nonlinear compressibility effects arising in the low transonic flow regime. In fact, once the critical Mach number is exceeded, the wave contribution to the global drag coefficient is no longer negligible. As a result, the difference in the quantity of interest, i.e. the aerodynamic efficiency, becomes important. This is presented in Fig. 5(b), where the relative error between the estimates of the two solvers is plotted in the range of Mach number and angle of attack dictated by the uncertainty on the induced velocity and blade pitch angle. Finally, the computational cost associated with the low-fidelity model is lower than the cost of the high-fidelity model: on average, the XFOIL solver is ten times faster than MSES.

C. Shape parameterization

The shape of the airfoil is the design output of the optimization problem. To define a finite, sufficiently small set of design variables, a parameterization is required. In this work, the Class/Shape function Transformation (CST)[49] is employed to describe the airfoil shape.

1. *Class/Shape function Transformation*

The parameterization is well-defined by specifying two functions: a geometry class function C and a shape function S that defines the particular shape of the geometry. The former is defined as follows

$$C(\psi) = \psi^{N_1}(1-\psi)^{N_2}, \tag{3}$$

where ψ is the non-dimensional chordwise coordinate ($\psi = x/c$) and N_1 and N_2 are appropriate coefficients that determine the class of the geometry; in the case of an airfoil with a rounded nose and a sharp trailing edge: $N_1 = 0.5$ and $N_2 = 1$ (see Ref.[49] for further details). The shape function $S(\psi)$ is given by a Bernstein polynomial of order n. The CST is applied to the camber mean-line ζ_c and to the thickness distribution ζ_t of the airfoil (both obtained by projection in the direction orthogonal to the x-axis) and it reads

$$\begin{aligned}
\zeta_c(\psi) &= C(\psi)\ S(\psi) + \psi\ \zeta_{TE_c} = C(\psi) \cdot \sum_{i=0}^{n} A_i^c S_{n,i}(\psi) + \psi\ \zeta_{TE_c} \\
\zeta_t(\psi) &= C(\psi)\ S(\psi) + \psi\ \zeta_{TE_t} = C(\psi) \cdot \sum_{i=0}^{n} A_i^t S_{n,i}(\psi)
\end{aligned} \tag{4}$$

where the coefficients A_i^c, A_i^t define the Bernstein polynomial coefficients of the camber line and thickness distributions respectively, $S_{n,i}$ is the i-th term of the Bernstein polynomial of order n defined as:

$$S_{n,i} = \frac{n!}{i!(n-i)!}\ \psi^i \cdot (1-\psi)^{n-i}. \tag{5}$$

The coordinate of the trailing edge of the mean camberline is ζ_{TE_c}, whereas the coordinate of the trailing edge of the thickness distribution ζ_{TE_t} is set to zero in order to consider closed trailing edge airfoils. Finally, from the meanline and camber distribution the upper surface ζ_u and lower surface ζ_l are computed as follows

$$\zeta_u(\psi) = \zeta_c(\psi) + \frac{1}{2}\zeta_t(\psi), \qquad \zeta_l(\psi) = \zeta_c(\psi) - \frac{1}{2}\zeta_t(\psi). \tag{6}$$

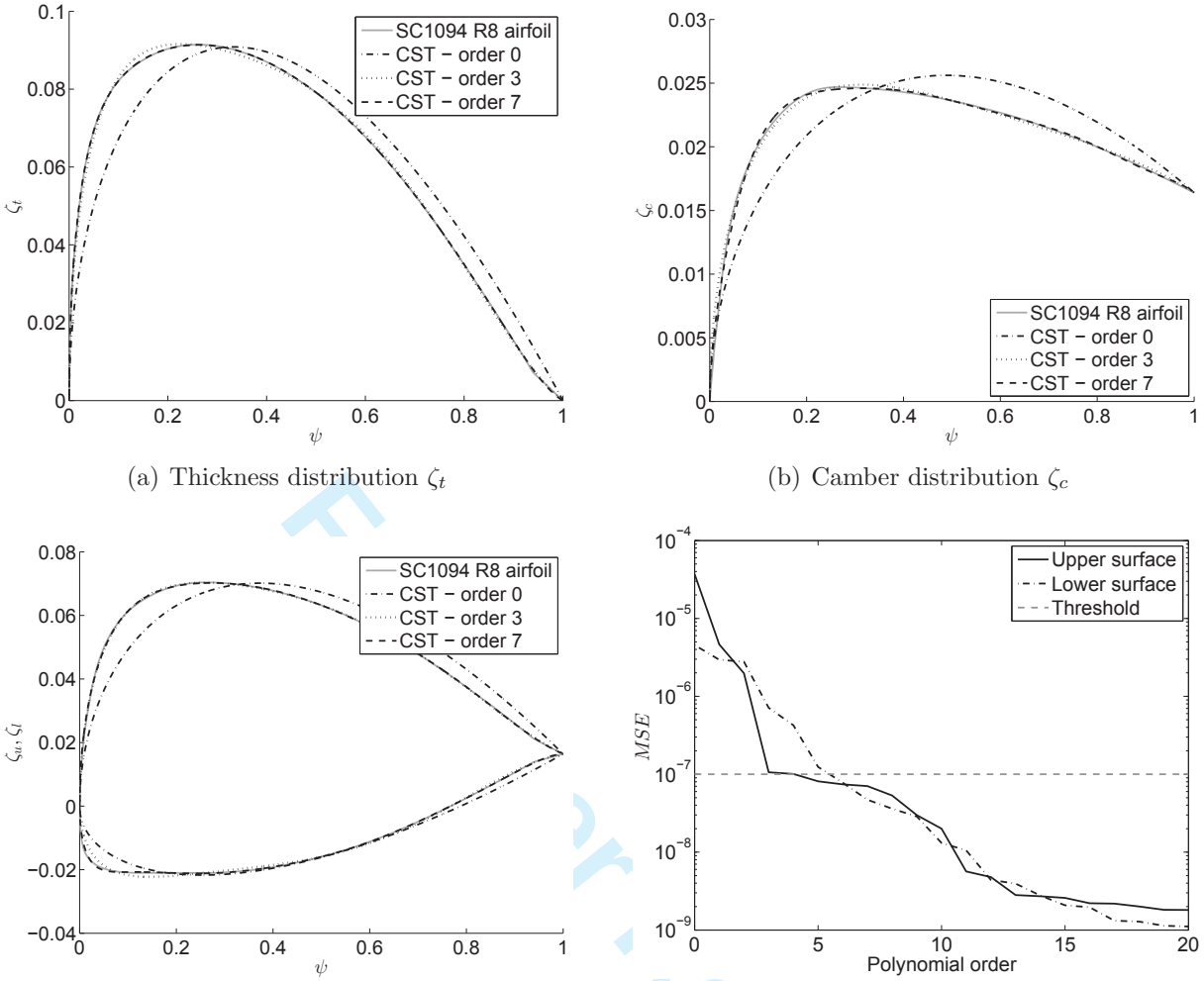

(a) Thickness distribution ζ_t

(b) Camber distribution ζ_c

(c) Resulting upper surface ζ_u and lower ζ_l surface

(d) Mean squared error MSE for upper and lower surfaces with increasing polynomial order

Figure 6. Results of the application of the CST for the SC1094 R8 airfoil: each dash-dotted line in (a), (b) and (c) corresponds to a given polynomial order.

2. Convergence analysis of the CST

The order of the polynomial is chosen based on a convergence analysis of the CST. To do this, the parameterization has been applied with an increasing polynomial order to represent a group of helicopter rotor airfoils (e.g. NACA23012, SC1095, SC1094, HH02). A least squares fitting is employed to determine the coefficients of the CST which best represents each airfoil. The mean squared error MSE is computed as follows

$$MSE = \frac{1}{n_p} \sum_{i=1}^{n_p} \left(\tilde{\zeta}_i - \zeta_{CST_i} \right)^2,$$

where n_p is the number of points on the airfoil surface, $\tilde{\zeta}_i$ is the exact airfoil and ζ_{CST_i} is the CST representation, both evaluated at the i-th point. The analysis proves that with a polynomial of 7-th order the mean quadratic error of the CST reaches a value equal to or lower than a desired threshold set to 10^{-7}. A representative set of results is shown for the airfoil SC1094 R8 in Fig. 6. Thus, the order of the polynomial is set to seven and the resulting design variables are 17: $\mathbf{y} = \{A_i^c, A_i^t, \zeta_{TE_c}\}$ with $i = 0, ..., 7$.

D. Optimization method

In the present work, the optimizer is based on the Nondominated Sorting Genetic Algorithm (NSGA),[50] that has been largely used by the authors in previous works (see for example Ref.[51] for more details). Main tuning parameters of the algorithm are the population size, the number of generations, the crossover and mutation probabilities *pc*, *pm* and the so-called sharing parameter r used to take into account the relative isolation of an individual along a dominance front. Typical values for *pc*, *pm* are, respectively, 0.9 and 0.1; values of r are defined following a formula given in Ref.[50] that takes into account the population size and the number of objectives. Finally, the constraint on the pitching moment is obtained by means of a penalty function that is applied to the lift-to-drag ratio when the moment coefficient exceeds the maximum value mentioned in Section II.

E. Uncertainty quantification

The goal of uncertainty quantification in this problem is to measure the statistics of the performance $E(\mathbf{y}, \boldsymbol{\xi})$ which depends on the uncertain input data $\boldsymbol{\xi}$ through the solution of Eq. (1). The propagation of the uncertainty from the uncertain input variables to the output of interest is discussed in the following.

1. Probabilistic framework

A probabilistic framework is employed to deal with the uncertain input data. In this context the stochastic input quantities $\boldsymbol{\xi}$ are treated as independent continous random variables. The random vector $\boldsymbol{\xi}$, whose dimension is equal to the number of uncertain variables n_ξ, belongs to the probability space $(\Omega, \mathcal{F}, P)$, composed by the sample space Ω, the σ-algebra $\mathcal{F}$ of the subsets of the events and a probability measure P. It essentially maps the samples in $\Omega = [0,1]^{n_\xi}$ into the random outcomes $\boldsymbol{\xi} \in \Xi$ and it is characterized by the probability density function $p_\xi(\boldsymbol{\xi})$. The output of the system, i.e. the solution of Eq. (1), is therefore a stochastic variable, and hence the performance $E(\mathbf{y}, \boldsymbol{\xi})$, which is a function of the solution, is a stochastic variable as well. In the robust optimization procedure the goal is to reconstruct the mean value and the variance of the quantity of interest; in the following, the stochastic

output variable is referred to as $u(\mathbf{y}, \boldsymbol{\xi})$, while its deterministic realization is $\tilde{u}_i(\mathbf{y}, \boldsymbol{\xi}_i)$. Let us define the expected value of the stochastic variable u as follows

$$\langle u \rangle = \int_{\Xi} u(\mathbf{y}, \boldsymbol{\xi}) \; p_{\xi}(\boldsymbol{\xi}) \; \mathrm{d}\xi,$$

with $p_{\xi}(\boldsymbol{\xi}) = \prod_i^{n_\xi} p_{\xi_i}(\xi_i)$ the joint probability of the independent input variables, and the inner product operator of two stochastic variable u and v with respect to the joint probability

$$\langle u, v \rangle = \int_{\Xi} u(\mathbf{y}, \boldsymbol{\xi}) v(\mathbf{y}, \boldsymbol{\xi}) \; p_{\xi}(\boldsymbol{\xi}) \; \mathrm{d}\xi.$$

The mean and variance then read

$$\begin{aligned} \mu(u) &= \langle u \rangle \\ \sigma^2(u) &= \langle u, u \rangle - \langle u \rangle^2. \end{aligned} \tag{7}$$

To compute the quantities in Eq. (7) several methods are available which are mainly divided into two categories: non-intrusive methods, which rely only on a set of samples of the output of the system, and intrusive methods, which instead require a manipulation of the equations of the system.[25] The first category is chosen because these methods do not require a modification of the numerical solver used to compute the solution $\mathbf{q}$ of Eq. (1) and thus the output u, and they also enable an easy coupling with the NSGA. Among these methods, the quasi Monte Carlo method and the polynomial Chaos expansion are discussed.

2. Quasi Monte Carlo method

The first method considered here is a sampling technique, the quasi-Monte Carlo (QMC) method. In this case, repeated simulations of Eq. (1) are required for each sample in the stochastic space to get the realizations $\tilde{u}_i$; the integrals in Eq. (7) are then replaced by an appropriate numerical quadrature. QMC differs from the usual Monte Carlo simulation in that it uses quasi-random sequences instead of pseudo random numbers. The quasi-random sequences are the low discrepancy Sobol sequences, which are deterministic and fill the space more uniformly than pseudo random sequences. This method has several advantages: it is simple and it does not rely on the regularity of the output of Eq. (1) with respect to the uncertain input [25, p. 8-9]. On the other hand, the rate of convergence scales with $n_s^{-1/2}$ with n_s the number of samples, thus a significant number of realizations are required to achieve a sufficiently good estimate of the statistical moments. This issue is of paramount importance for fluid dynamics applications, because the computation of Eq. (1) is typically very expensive.

3. Polynomial Chaos expansion

The employment of the Polynomial Chaos (PC) expansion can reduce the computational cost of the uncertainty propagation, especially when a small number of uncertain variables are considered, although it relies on the regularity of the function u in the stochastic space. In fact, under specific conditions, a stochastic process can be expressed as a spectral expansion based on suitable orthogonal polynomials, with weights associated to a particular probability density function. The first study in this field is the Wiener process that was later developed in Ref.[52] The basic idea is to project the variables of the problem onto a stochastic space spanned by a complete set of orthogonal polynomials Ψ that are functions of the random variables $\boldsymbol{\xi}$. For example, variable u has the following spectral representation:

$$u\left(\mathbf{y},\boldsymbol{\xi}\right)=\sum_{k=0}^{\infty}\alpha_k\left(\mathbf{y}\right)\Psi_k\left(\boldsymbol{\xi}\right). \tag{8}$$

where Ψ_k are the PC orthogonal polynomials and α_k the coefficients of the expansion. In practice, the series in Eq. (8) has to be truncated to a finite number of terms N, which is determined by

$$N+1=\frac{(n_\xi+n_o)!}{n_\xi!\;n_o!},$$

where n_ξ is the dimension of the uncertainty vector $\boldsymbol{\xi}$ and n_o is the order of the univariate polynomial expansion $\phi_i(\xi_i)$ from which the multivariate polynomials $\Psi_k(\boldsymbol{\xi})$ are obtained via tensorization, i.e.

$$\Psi_k\left(\boldsymbol{\xi}\right)=\prod_{i}^{n_\xi}\phi_i(\xi_i).$$

The polynomial basis $\phi_i(\xi_i)$ is chosen according to the Wiener-Askey scheme[52] in order to select orthogonal polynomials with respect to the probability density function $p_\xi(\boldsymbol{\xi})$ of the input. In this work, because a uniform distribution is considered, Legendre polynomials are employed. The orthogonality property can be advantageously used to compute the PC coefficients of the expansion α_k in a non-intrusive PC framework; this procedure is called Non-Intrusive Spectral Projection (NISP).[51] In fact, from the orthogonality property it directly follows that

$$\alpha_k=\frac{\langle u(\mathbf{y},\boldsymbol{\xi}),\Psi_k(\boldsymbol{\xi})\rangle}{\langle\Psi_k(\boldsymbol{\xi}),\Psi_k(\boldsymbol{\xi})\rangle}\qquad\forall k. \tag{9}$$

The computation of the PC coefficients requires the integration of the polynomials in Eq. (9). This can be estimated with several approaches, among which Gaussian quadrature formula is chosen in this study.[51] As a result, the solution of the deterministic problem in Eq. (1) is required for each quadrature point. Once the polynomial chaos and the associated α_k coefficients are computed, the mean value and the variance of the stochastic solution $u\left(\mathbf{x},\boldsymbol{\xi}\right)$

are obtained by leveraging the orthogonality of the polynomials Ψ_k with respect to the probability function p_ξ:

$$\mu(u)|_{PC} = \left\langle \sum_{k=0}^{N} \alpha_k(\mathbf{y})\,\Psi_k(\boldsymbol{\xi}) \right\rangle = \alpha_0(\mathbf{y})$$

$$\sigma^2(u)|_{PC} = \left\langle \left(\sum_{k=0}^{N} \alpha_k(\mathbf{y})\,\Psi_k(\boldsymbol{\xi}) \right)^2 \right\rangle - \alpha_0^2(\mathbf{y})$$

$$= \sum_{k=1}^{N} \alpha_k^2(\mathbf{y}) \left\langle \Psi_k^2 \right\rangle .$$

4. Convergence study of PC order

Before running the robust optimization, a preliminary convergence study in the stochastic space was performed to determine the number of deterministic computations required for each design run. Thus, the QMC and PC methods are employed to reconstruct the mean and variance of the lift-to-drag ratio for the NACA 0012. For this comparison, the MSES code for the section at 40% of the blade radius is considered. Results are presented in Fig. 7, where mean and variance are plotted against the order n_o of the polynomials employed by the PC method. Note that the number of samples employed by the PC approach is $(n_o+1)^{n_\xi}$, whereas the number of samples for the QMC method are indicated in brackets in the legend of the figure. The comparison shows that the PC results tend to reach the QMC result corresponding to the higher number of evaluations (1000) with an increasing

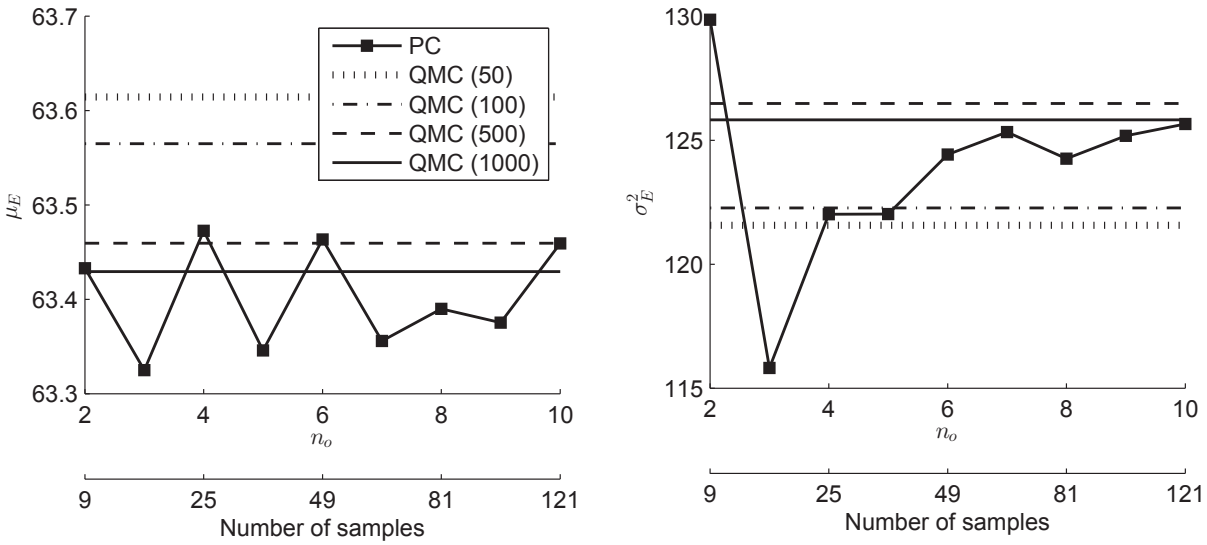

Figure 7. Estimate of the mean value (left) and variance (right) of the lift-to-drag ratio E obtained with QMC and PC methods.

Table 4. Results of convergence study with QMC and PC methods (the percentage error is computed with respect to the value obtained with QMC with 1000 samples.

	Samples	μ_E	Error μ_E [%]	σ_E^2	Error σ_E^2 [%]
QMC	50	63.6145	0.29	121.5720	3.38
	100	63.5651	0.21	122.2711	2.82
	500	63.4597	0.05	126.4798	0.52
	1000	63.4296	-	125.8205	-
PC	9	63.4331	0.01	129.8617	3.21
	16	63.3252	0.16	115.8137	7.95
	25	63.4729	0.07	122.0178	3.02
	36	63.3460	0.13	122.0256	3.02
	49	63.4635	0.05	124.4259	1.11
	64	63.3561	0.12	125.3327	0.39
	81	63.3902	0.06	124.2543	1.25
	100	63.3755	0.09	125.1795	0.51
	121	63.4595	0.05	125.6586	0.13

PC order. Taking the QMC result with 1000 samples as a reference, the percentage errors on the mean err(μ_E) and the variance err(σ_E^2) are computed. The error on the mean value is far below 1%, whereas for the variance, a PC order equal to or higher than four is required to get an error lower than 4% (see Tab. 4). Given these results, the fourth-order PC, which corresponds to 25 samples per design, is chosen for the optimization, as it represents a good trade-off between accuracy and computational cost. This analysis proves the capability of the PC approach to provide an accurate estimate of the statistics with a much lower number of samples with respect to the Monte Carlo method for the problem of interest. It is also worth noting that a higher number of samples are required to get a higher order statistical moment (i.e. the variance), whereas the mean value is well-estimated with fewer terms.

IV. Multi-fidelity strategy based on physical models

From the scheme outlined in Fig. 3 it is evident that the coupling of the optimization loop with the uncertainty quantification analysis results in a substantial increase of the computational cost of the optimization procedure. This increase is due to the higher number of evaluations of the solution of Eq. (1) required by the uncertainty propagation technique. It is therefore proportional to the cost of solving the system equations. In the case of a low-fidelity model, which is typically fast or moderately expensive, the global optimization cost is still feasible, but it becomes less attractive when more accurate, yet expensive models

are available. The employment of an inappropriate aerodynamic model inevitably affects the estimate of the objective function: inaccurate estimates, such as those obtained with a low-fidelity model, may drive the optimization procedure to false optima. To possibly circumvent this problem while reducing the computational cost, a multi-fidelity optimization algorithm is proposed which employes information coming from both the low-fidelity and high-fidelity models.

A. Description of the multi-fidelity strategy

The starting point is the definition of two models of different fidelity, each of which balances out the other's cons. An initial characterization of the discrepancy between the estimates of the models must be performed. To do this, the quantity of interest for a reference design is computed with both models in each point of the sampling set Ω_s in the stochastic space defined by the UQ non-intrusive method. The reference design is either the initial design or a design representative of the class of possible solutions defined by the chosen parameterization. Then, a set Ω_c of *control points* is defined which represents a subset of the samples set Ω_s in the stochastic space. This subset includes some representative samples of the difference between the two models; for example, the sample corresponding to the nominal condition, the samples with highest and lowest discrepancy in each dimension of the stochastic space may fall into this subset. In the optimization loop, the control points for each design will be evaluated with both models, to measure the difference between them. The neighbouring sample points will be evaluated with either the low or high-fidelity model according to a switching logic based on the discrepancy of the closest control point.

For the problem considered here, the switching logic relies on physical considerations based on compressibility effects. In fact, the approach used to discriminate the quality of the results is based on the hypothesis that the low-fidelity model provides an adequate estimate of the performance unless significant compressibility effects are present. When compressibility is not negligible, the method switches from the low-fidelity model to the high-fidelity model to get a more accurate estimate of the objective function. As a result, the high-fidelity model is used only for a small number of samples, namely the samples in which the freestream Mach number exceeds the critical value as shown in Fig. 5(a). However, the operating conditions for the onset of significant compressibility effects depend on the shape of the airfoil, and thus they should be evaluated for each particular design in the optimization loop. For this reason, it is necessary to decide, independently for every design configuration, which model to use for each of the 25 samples in the domain Ω_s required by the PC expansion. First, the subset Ω_c of control points is defined, which includes the limiting operating conditions in the stochastic space. Because the physical problem considered here is dominated by the effect of the angle of attack and the Mach number, the samples $\boldsymbol{\xi}_i$ are mapped into the (α, M)-plane.

The subset of control points is chosen as the set of conditions including (i) the nominal condition (α_n, M_n), and the conditions corresponding to the bounds of the complete samples set: (ii) minimum Mach number M_{min} and angle of attack at the minimum Mach number $\alpha_{M_{min}}$, (iii) maximum angle of attack α_{max} and minimum Mach number M_{min}, (iv) maximum Mach number M_{max} and minimum angle of attack α_{min}, (v) maximum Mach number M_{max} and angle of attack at maximum Mach number $\alpha_{M_{max}}$ (see the crosses in Fig. 8). Once the control points are defined, a measure of the compressibility effects is required as a control function. The discrepancy between the low-fidelity model and the high-fidelity model is chosen, because this difference is strictly connected to the increase of the wave drag, as presented in Section III . B. For each individual in a generation, the following steps are performed (summarized in Fig. 9):

1. compute the performance using the low-fidelity model J_l and using the high-fidelity model J_h for the control points and evaluate the control function $\mathcal{C}$ for each control point

$$\mathcal{C}_i = |(J_{h,i} - J_{l,i})/J_{h,i}| \quad \forall i \in \Omega_c,$$

   which represents the error of the low-fidelity estimate;

2. for each sample point $j \in \Omega_s$, the closest control point $i \in \Omega_c$ is computed and if the control function $\mathcal{C}_i$ for such control point exceeds an assigned threshold value τ, the solution of Eq. (1) is evaluated with the high fidelity model, otherwise, the low-fidelity estimate is employed;

3. the mean value and variance are computed by means of the uncertainty quantification method using the samples in Ω_s.

As a result, some samples in the stochastic space are evaluated with the low-fidelity model, and others with the high-fidelity model (see Fig. 8).

The method is independent of the type of sampling in the stochastic space, and of the input PDF as well. However, it is strongly influenced by the choice of control points. In this case five control points have been chosen. Additional intermediate control points can be used to improve the resolution of the control function. This may be a good strategy in the case of control functions that have many local minima/maxima. It could reduce the number of HF samples for a given design, but it would increase the number of HF computations required by the switching logic. A trade-off number should be found, which may also take into account the available resources. A physical knowledge of the problem under consideration and of the models employed in the optimization would support the definition of the control points in the multi-fidelity strategy.

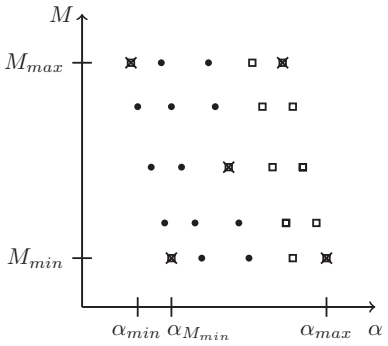

	α	M
i	α_n	M_n
ii	$\alpha_{M_{min}}$	M_{min}
iii	α_{max}	M_{min}
iv	α_{min}	M_{max}
v	$\alpha_{M_{max}}$	M_{max}

Figure 8. Points used in the multi-fidelity strategy in the (α, M)-plane; the quadrature points are divided into: control points (cross), points evaluated by the low-fidelity model (filled dots) and points with significant compressibility effects evaluated with the high-fidelity model (empty squares). Summary of the control points on the right.

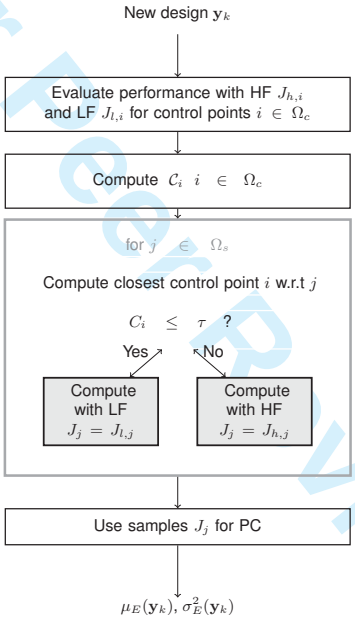

Figure 9. Flowchart of the multi-fidelity selection strategy.

To some extent, this multi-fidelity method could be regarded as an extension of an Evolution Control strategy[53] in the case of uncertainty-based optimization. As a matter of fact, Evolution Control is a multi-fidelity technique for evolutionary algorithms in which either a certain number of individuals within a generation or a certain number of generations within an evolution are evaluated with the high-fidelity fitness function. The "control" consists in switching to the higher fidelity method for those selected individuals, thereby adding high-fidelity information about the fitness function of the population. In the application to robust

optimization, the proposed method performs a control of the evolution in the stochastic space rather than in the design space. In other words, the switching logic acts on each individual of every generation, but only for a subset of samples in the stochastic space.

B. Preliminary results

The multi-fidelity strategy is applied to the NACA 0012 as a reference configuration. The PC meta-model which represents the system output E as a function of the uncertain variables (i.e. induced velocity V_i and blade pitch angle θ), is obtained by means of the high-fidelity (HF) model, the low-fidelity (LF) model and finally with the proposed multi-fidelity (MF) strategy. The result is presented in Fig. 10, where the samples of the PC method are marked

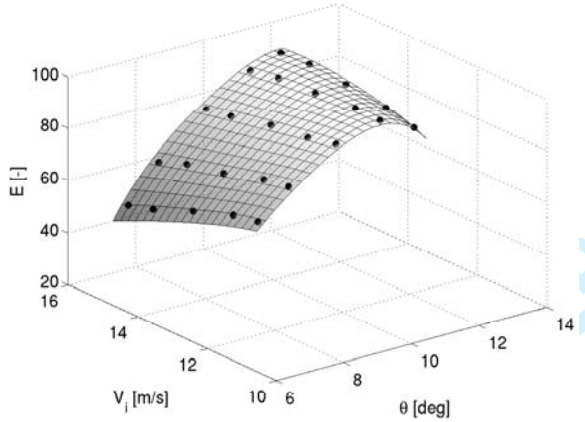

(a) Efficiency meta-model obtained with LF samples

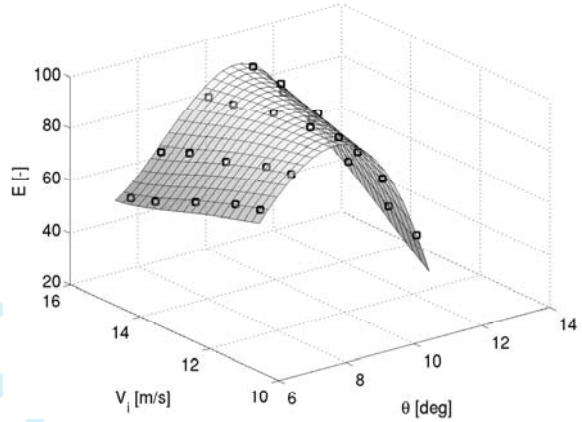

(b) Efficiency meta-model obtained with HF samples

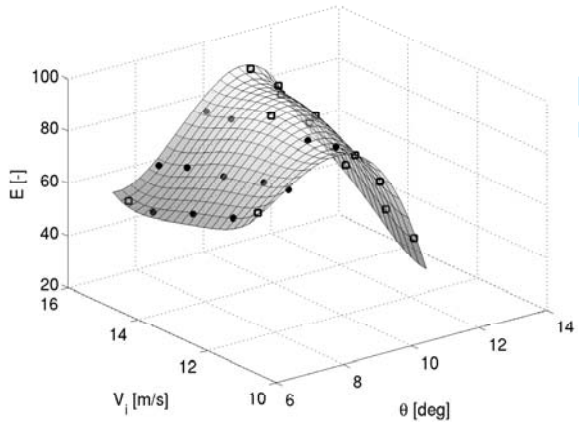

(c) Efficiency meta-model obtained with MF samples

Figure 10. Aerodynamic efficiency evaluation on the PC sampling points using the multi-fidelity approach (empty squares for HF samples, filled dots for LF samples) at $r = 0.8$.

as squares when the HF estimate is employed and dots for the LF computations. As expected, the LF model does not account for the loss in the aerodynamic efficiency encountered at higher values of pitch angles and low values of induced velocity (which correspond to higher angles of attack, since the induced velocity acts as a downwash on the airfoil flowfield). Instead, the correction of the MF method, which is mainly applied in that area, yields the quantitative behavior of the response obtained with the HF model. The statistics resulting from the PC expansion are then collected in Table 5, which presents the mean value, variance and probability of the efficiency E obtained with the HF method and the relative error obtained with the LF model and MF strategy. The error on the MF estimates of the function employed in the optimization loop are reduced with respect to the LF case. Figure 11 shows the Probability Density Function (PDF) of the lift-to-drag ratio obtained by means of Monte Carlo sampling of the PC meta-model. It appears that the multi-fidelity strategy well captures the tail of the distribution and it shares the same support with respect to the high-fidelity PDF, although both the low-fidelity and the multi-fidelity models lack accuracy

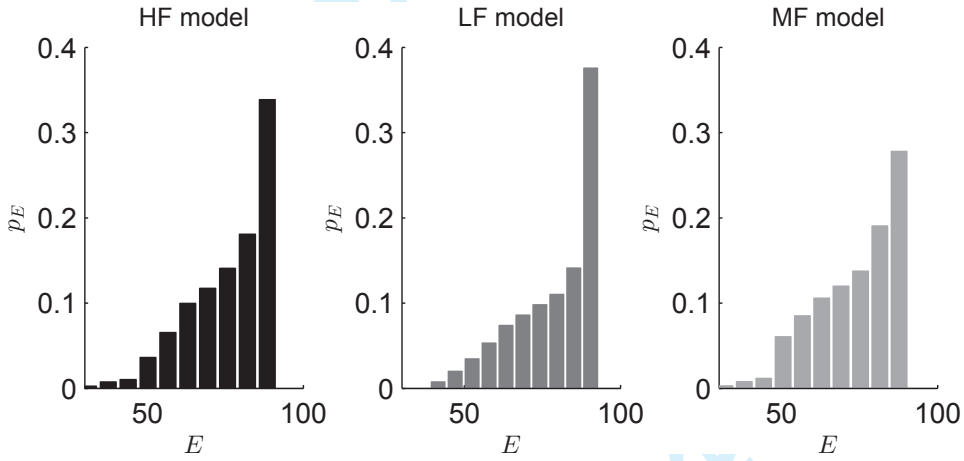

Figure 11. Comparison of uncertainty output prediction of the high fidelity (HF) method, low fidelity (LF) method and multi-fidelity (MF) method at $r = 0.8$.

Table 5. Reconstruction of statistics with low-fidelity, high-fidelity and multi-fidelity models at $r = 0.8$.

Method	μ	σ^2	σ/μ	$p(E < 50)$	$p(50 \leq E \leq 80)$	$p(E > 80)$
HF	74.89	128.99	0.15	0.03	0.54	0.43
	err (μ)	err (σ^2)	err (σ/μ)	err $(p(E < 50))$	err $(p(50 \leq E \leq 80))$	err $(p(E > 80))$
LF	3.92 %	6.77 %	0.56 %	20.97 %	17.28 %	22.93 %
MF	3.02 %	0.68 %	3.46 %	4.12 %	13.08 %	16.64 %

in predicting the PDF peak.

Furthermore, the estimates of the mean value and variance of the aerodynamic efficiency obtained with the HF, LF and MF optimization strategies are compared for the set of 200 individuals belonging to the first generation of the genetic algorithm for the blade section at 80% of the radius. The estimates are non-dimensionalised and plotted in Fig. 12, where the dispersion with respect to the solid line represents the error between the method reported on the ordinate and the HF result on the abscissa. The MF strategy greatly reduces the dispersion of the LF results, demonstrating the effectiveness of the switching logic.

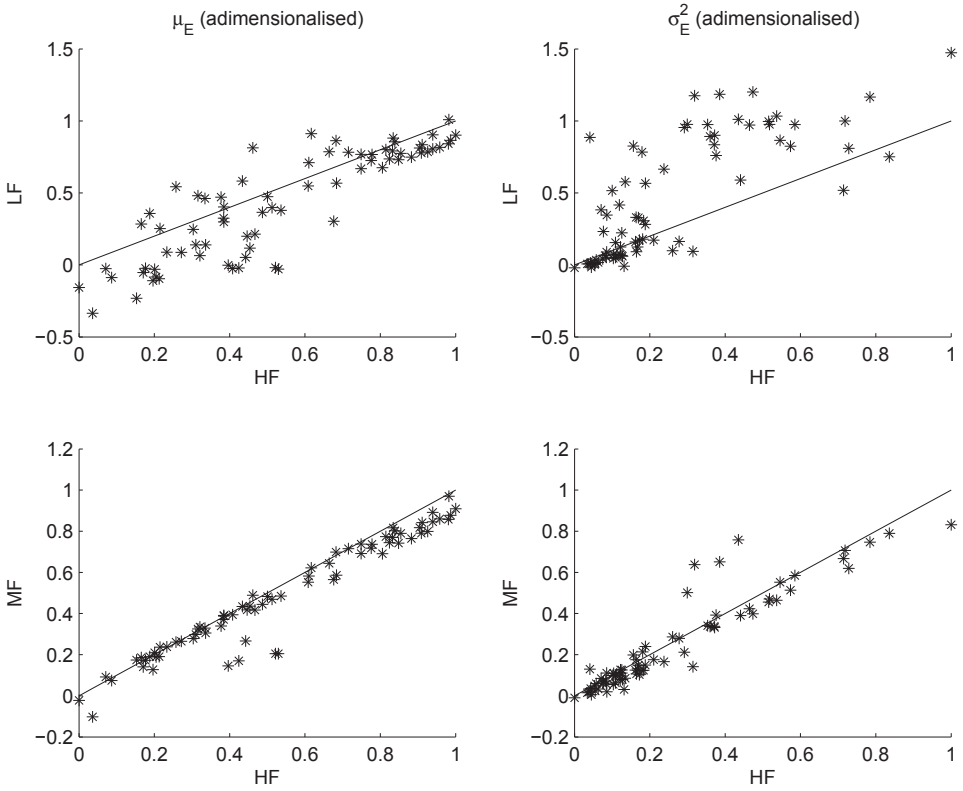

Figure 12. Comparison of objective estimates of the HF, LF and MF methods for the first generation of the robust genetic optimization obtained at $r = 0.8$.

V. Optimization results

Two blade sections are considered: an inboard section at 40% of the blade radius and an outboard section at 80% (the corresponding operating conditions are reported in Table 2). The operating Mach number of the blade section in this case is mainly affected by the tangential velocity due to the rotor rotation, which grows linearly going outboard. Thus, the inboard section features subsonic flow, whereas the outboard section undergoes low tran-

sonic flow. The results for the inboard section are presented to assess the effectiveness of the robust optimization technique by comparing the results with other classical optimization approaches, such as the deterministic single-point and multi-point optimization problems. The second set of results are aimed at presenting the performance of the multi-fidelity algorithm developed in this work.

A. Inboard section

In this section, the results of the optimization of the inboard section airfoil obtained with the low-fidelity model are presented in order to examine the effectiveness of the robust optimization approach. In addition, because the operating conditions at 40% blade span do not involve significant compressibility effects, the low-fidelity model in this condition provides good estimates of the quantity of interest at a very low computational cost.

1. *Convergence analysis of optimizer*

To begin with, some properties of the optimization algorithms are discussed. The population size and the number of generations for the convergence of the genetic algorithm should be chosen according to the number of parameters and objectives of the particular optimization problem. However, in practice the population size and number of generations are set by also taking into account the constraints related to the global amount of CPU time devoted to the computation. It must be recalled that taking too small a population may rapidly lead to a local optimum from which the iteration process on the generation number will not evolve. On the other hand, a large population would permit the computation of only a few generations, resulting in a poorly converged solution. In the present work, after performing an initial generation of 200 individuals to explore the design space, 40 individuals are then retained and evolved. The evolution of the Pareto front is presented in Fig. 13(a), where the objective functions of the individuals are presented at different generations. It appears that by increasing the number of generations the front moves to higher values of the mean and lower values of the variance, with a decaying rate.

To assess the convergence of the genetic optimization, several empirical measures are available: the global number of dominated solutions per generation, the diversity or spread of the individuals in the design space and the domination rate.[54,55] The latter measure represents the percentage of non-dominated individuals that become dominated in the following generation, and should then decrease as the population evolves. The aforementioned domination rate is plotted in Fig. 13(b). Despite the presence of oscillations due to the stochastic nature of the genetic algorithm, the convergence trend is still clear.

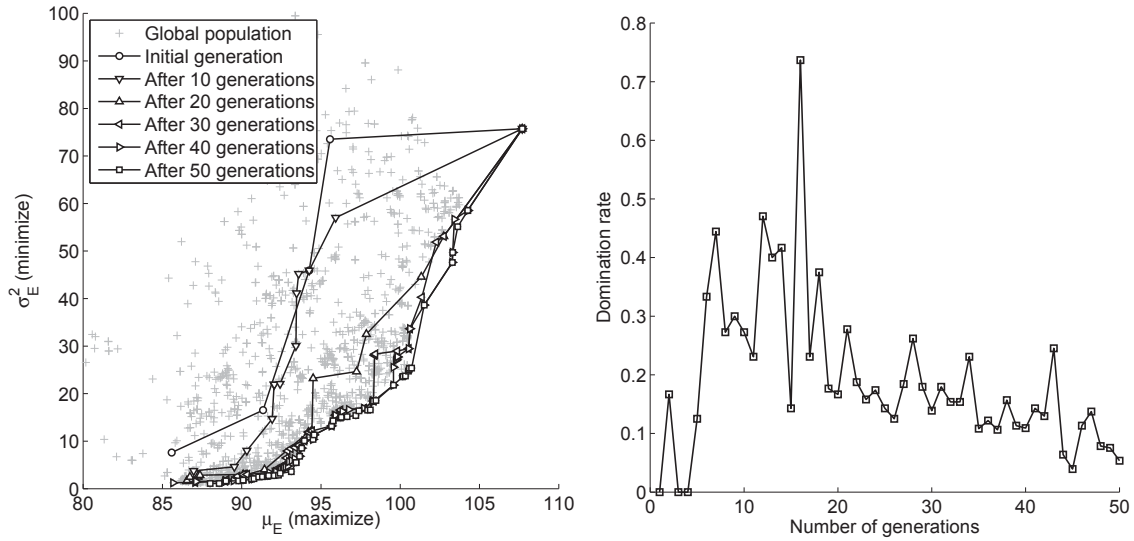

(a) Pareto front evolution (b) Domination rate

Figure 13. Convergence of the Pareto front (LF method).

2. *Analysis of Pareto fronts*

The final Pareto front is shown in Fig. 14(a), where the optimal mean airfoil and the optimal variance airfoil are highlighted with different symbols. Estimates of the mean and variance for selected reference airfoils are compared against the Pareto front in the same figure. The NACA 23012 has been here analysed, since it is a reference airfoil for rotorcraft applications. The airfoil labelled Single-Point is the optimal airfoil obtained with a single-objective deterministic optimization in the nominal operating condition. Likewise, the Multi-Point airfoil is the result of a multi-point single-objective optimization, where the cost function is the average sum of the lift-to-drag ratio over three operating conditions (nominal, higher angle of attack and lower angle of attack conditions). For these airfoils, the statistics have been evaluated in a post-processing phase by computing the aerodynamic efficiency in the same uncertain conditions employed for the robust approach. In the objective space, the reference airfoils have either a high mean value (NACA 23012, Single-Point and Multi-Point) or a low variance (NACA 0012). The non-dominated solutions represent a trade-off between the two requirements: in fact, they have a high mean value comparable to those of the Single-Point airfoil, but they also have a variance lower than the value of the NACA0012. In this sense, they outperform the reference airfoils. This is especially true in terms of robustness (i.e. reduction of the variance), even for the cases where the maximum mean values of the efficiency are obtained. As a consequence, the robust approach appears to be a better design method, even when compared with the multi-point optimization. This is because it results in the enhancement of the performance indicators. The airfoils with higher mean and lower

variance and a representative trade-off airfoil lying close to the midpoint of the Pareto front are plotted in Fig. 14(b).

The results obtained with the high-fidelity and multi-fidelity methods are presented in Figs. 15(a) and 15(b). In order to compare the three fronts, the airfoils belonging to the LF and MF fronts have been post-processed with the HF model. Figure 16(a) shows the comparison of the Pareto fronts. The results obtained by means of both the low-fidelity and

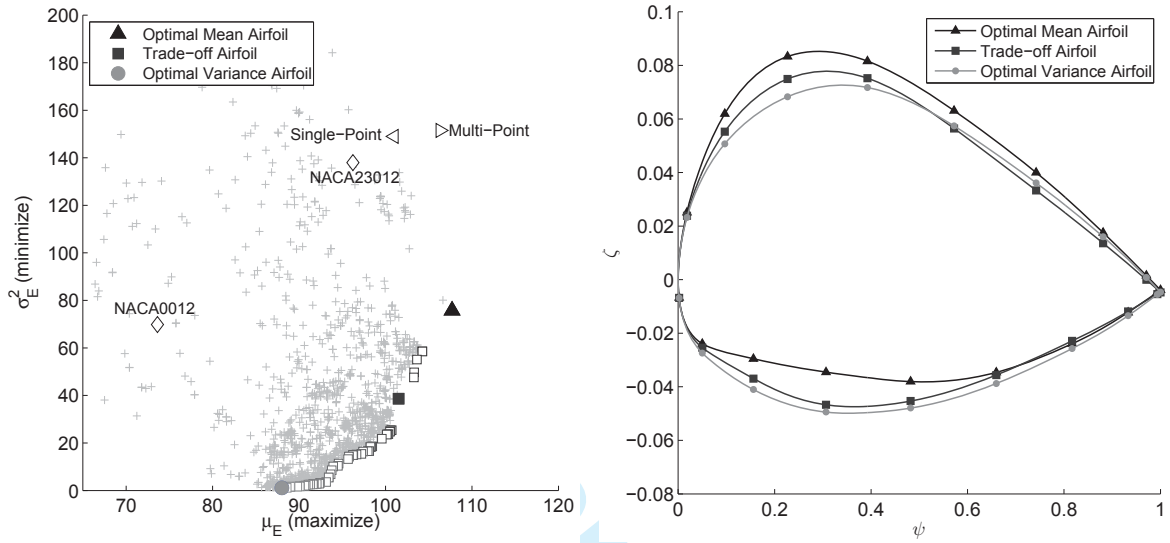

(a) LF Pareto front (b) LF Airfoils

Figure 14. Result of the optimization at $r = 0.4$ for the LF methods.

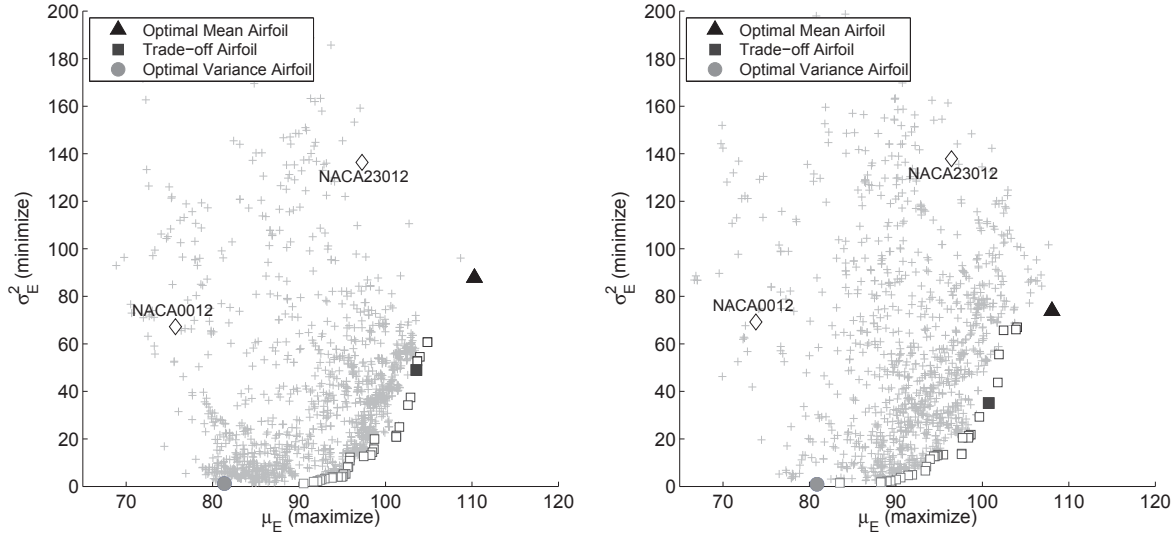

(a) HF Pareto front (b) MF Pareto front

Figure 15. Result of the optimization at $r = 0.4$ for the HF and MF methods.

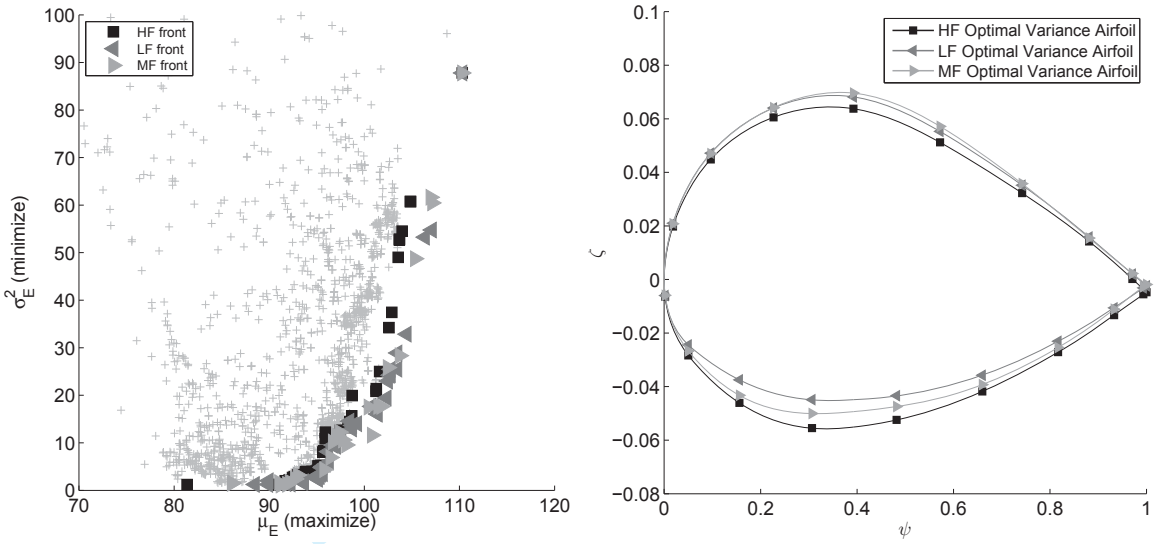

(a) Pareto fronts: the objectives of the airfoils belonging to LF and MF fronts are re-computed with the HF model for comparison

(b) LF, HF, MF Optimal Mean Airfoils

Figure 16. Comparison of LF, HF and MF results at $r = 0.4$.

multi-fidelity methods are in very good agreement with those of the high-fidelity model. In particular, the optimal mean airfoil is the same in the three cases, and the optimal variance airfoils are very similar (Fig. 16(b)). In fact, the basic physics that dominates the flow in this condition is captured in a similar way by the two numerical models. Nevertheless, the multi-fidelity result is closer to the low-fidelity one. Since the Mach number in this case does not exceed 0.258, the control of the multi-fidelity strategy acts only on a relatively small number of points, as defined in Section IV.

A quantitative measure of this difference is computed by taking the mean of the distance of each point of the Pareto front to the closest point of the HF Pareto front, as suggested in Ref.[56] In mathematical terms, the distance d_{A-B} of the Pareto set $\mathcal{P}_A$ to the Pareto set $\mathcal{P}_B$ reads

$$d_{A-B} = \frac{1}{|\mathcal{P}_A|} \sum_{i=0}^{|\mathcal{P}_A|} \min_{\mathbf{f} \in \mathcal{P}_B} ||\mathbf{f}(\mathbf{y}_i) - \mathbf{f}(\mathbf{y}_{\mathcal{P}_B})|| \tag{10}$$

where symbol $|\cdot|$ indicates the cardinality (i.e. number of elements) of the set, symbol $||\cdot||$ is the Euclidean distance, $\mathbf{f}$ and $\mathbf{y}$ are respectively the objective functions and the design variables of the elements in the Pareto set. The distance d_{MF-HF} of the MF set to the HF set is equal to 44.1, while the distance d_{MF-LF} of the MF set to the LF set is 4.4, proving that the MF set is closer to the LF set rather than the HF set (see Tab. 6). With regard to the computational cost, the number of function evaluations are computed to compare the

Table 6. Distance of MF front to HF and LF fronts for $r = 0.4$.

d_{MF-HF}	d_{MF-LF}
44.1	4.4

Table 7. Comparison of computational cost of different robust optimization strategies: cost is computed considering 1 cost unit for each HF evaluation and 0.1 cost unit for each LF evaluation.

	LF	HF	MF
LF evaluations	32100	-	31625
HF evaluations	-	32450	6325
Cost	3210	32450	9487

three strategies. In particular, the cost is computed by approximating the ratio of the cost of a single LF run over the cost of a HF run to 0.1 and the results are presented in Table 7. It is evident that the low-fidelity and the multi-fidelity strategy permit a great reduction of the computational cost, although the optimization result is still consistent with the high fidelity-based method.

3. *Analysis of optimal airfoils*

In the following, the optimal mean airfoil and the optimal variance airfoil obtained with the high-fidelity model are analysed in more detail. First, the meta-models representing the lift-to-drag ratio in the stochastic space are compared in Fig. 17(a). As expected from the optimization objectives, the lift-to-drag ratio of the optimal variance airfoil is almost constant over the domain at the expense of a poorer performance. The output PDF is then obtained by Monte Carlo sampling of the meta-model and it is presented in Fig. 17(b). The PDF of the optimal mean airfoil has a spread support which extends to higher values of the lift-to-drag ratio, whereas the PDF of the optimal variance airfoil is narrower.

The preceding figures have shown that the optimal variance airfoil appears to achieve the target of minimizing the variance, by reducing the peak of the aerodynamic efficiency with respect to the angle of attack. In order to do so, the optimization process leads to an airfoil shape that reduces the aerodynamic load, by unloading the region after the suction peak on the upper surface and by increasing the local curvature on the lower surface with respect to the optimal mean airfoil (see Fig. 18). The reduction of the upper surface thickness results in a sharper leading edge. The fast transition to a turbulent boundary layer induced by the highly loaded nose contributes to the reduction in the lift-to-drag ratio due to the increase

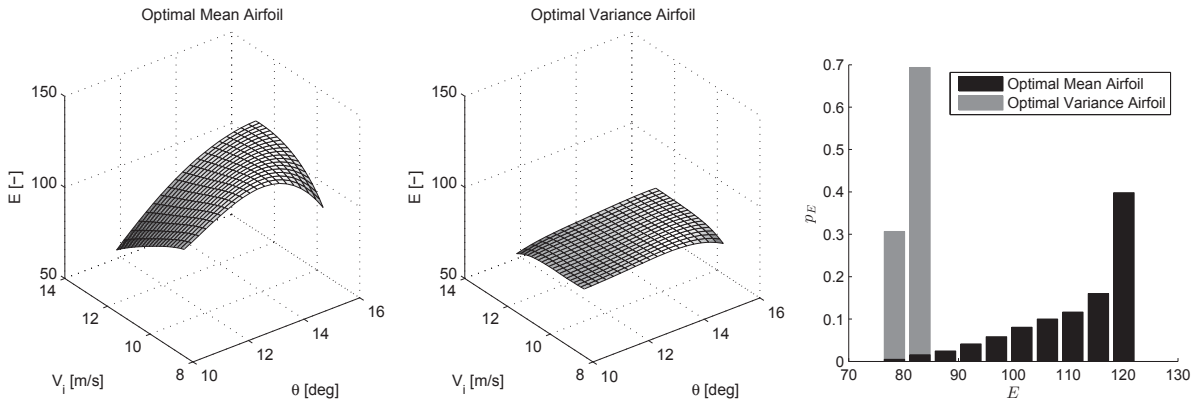

(a) Efficiency meta-model in the stochastic space (b) Sampled PDF of the efficiency

Figure 17. Efficiency of the optimal mean and variance airfoils (HF).

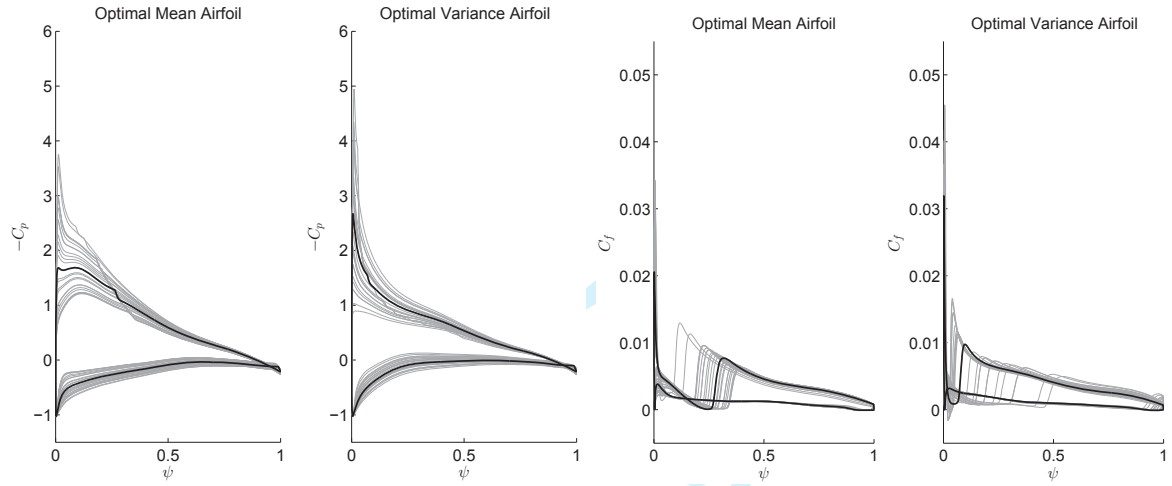

(a) Pressure coefficient (b) Friction coefficient

Figure 18. Comparison of the flowfield of the optimal airfoils (HF): a thick black line is employed for the nominal condition and thin grey lines for the remaining samples.

in friction drag. On the other hand, the optimal mean airfoil has higher camber with a more loaded upper surface and a nearly flat region on the lower surface to reduce the flow acceleration. In addition, the pressure peak at the leading edge is less severe and more gradual with respect to the optimal variance airfoil, moving towards a laminar flow airfoil. This results in a lower drag coefficient, at the cost of a higher sensitivity of the performance with respect to changes in the operating conditions. As a final remark, the optimal mean airfoil obtained in this optimization appears to be very similar to the result obtained in Ref.[7] for the subsonic lift optimization of an airfoil with constrained drag. However, the leading edge in that case is more drooped owing to the higher freestream angle of attack.

B. Outboard section

In the case of the outboard section at 80% of the blade radius, the freestream condition is low transonic and the compressibility effects are expected to result in non-negligible differences among the three optimization strategies.

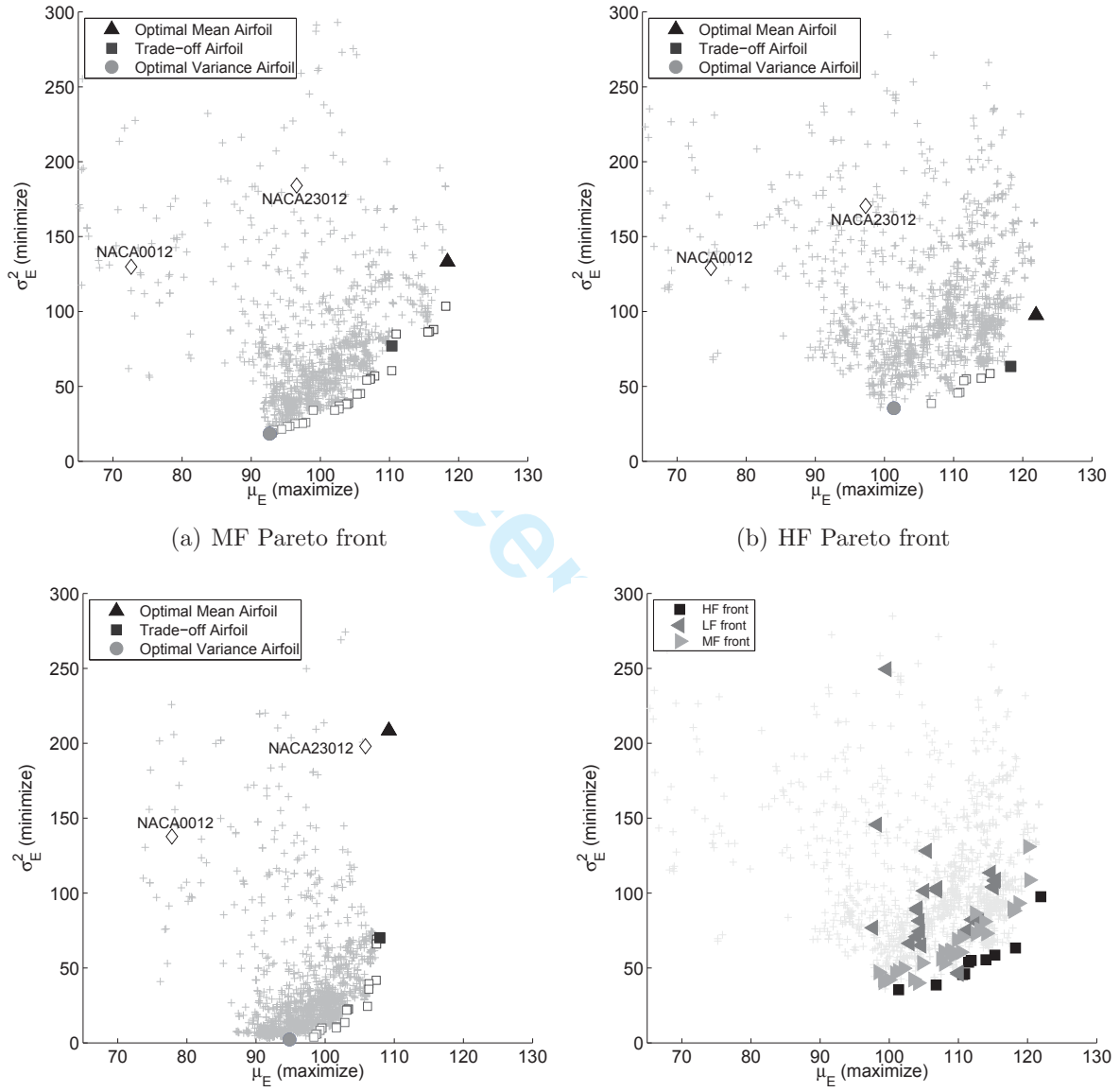

(a) MF Pareto front

(b) HF Pareto front

(c) LF Pareto front

(d) Pareto fronts: the objectives of the airfoils belonging to LF and MF fronts are re-computed with the HF model for comparison

Figure 19. Result of the optimization at $r = 0.8$.

1. *Analysis of Pareto fronts*

The Pareto front obtained with the proposed multi-fidelity strategy is presented in Fig. 19(a). The MF Pareto front is closer to the front obtained with the HF method (Fig. 19(b)), even though the starting point of the method is the full LF method which results in a very different front (Fig. 19(c)). To better appreciate the improvement of the MF method with respect to the LF optimization, the LF and MF fronts are re-computed with the HF model, and compared with the HF results in Fig. 19(d). The multi-fidelity result is closer to the HF result with respect to the LF front: using the definition in Eq. (10), the distance d_{MF-HF} of the MF set to the HF set is equal to 9.5, while the distance d_{LF-HF} of the LF set to the HF set is 22.8 (see Tab. 8). Also, the MF method defines a Pareto front on the objective space, whereas the LF results are more sparse and do not present a clear trend.

The airfoils obtained by the optimization are presented in Fig. 20. With respect to the mean optimal airfoils, although the MF and the HF results have a different maximum thickness position, they present similar curvature in the region close to the leading edge. Note that the LF optimal mean airfoil shows a greater leading edge radius, and a distribution of the lower side which resembles the airfoil obtained for the inboard section. As expected, the

Table 8. Distance of MF and LF fronts to HF front for $r = 0.8$.

d_{MF-HF}	d_{LF-HF}
9.5	22.8

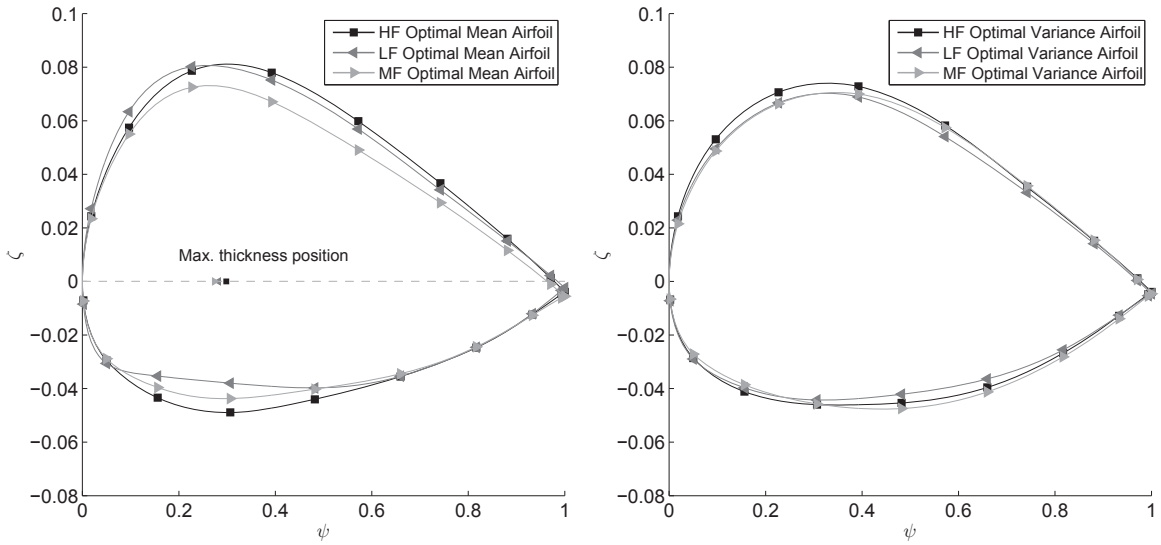

(a) LF, HF, MF Optimal Mean Airfoils (b) LF, HF, MF Optimal Variance Airfoils

Figure 20. Comparison of LF, HF and MF results.

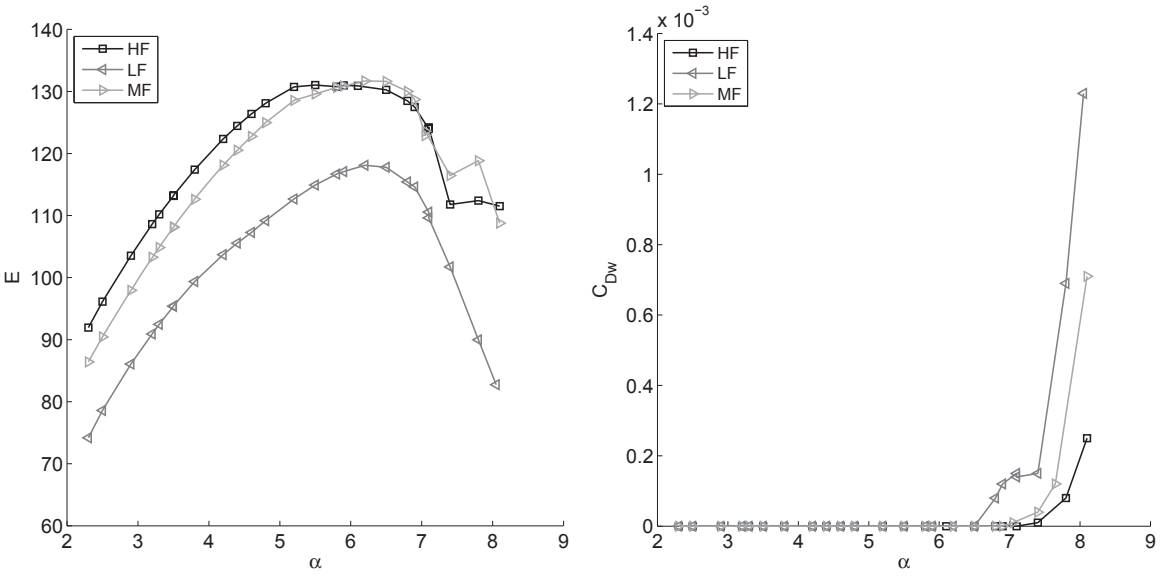

(a) Efficiency (b) Wave drag coefficient

Figure 21. Comparison of the performance and of the optimal mean airfoils resulting from LF, HF and MF methods: results of LF and MF optimizations are re-computed with HF model.

LF result does not take into account the change in the operating conditions. The difference on the optimal variance airfoils is instead less pronounced.

The performance of the mean optimal airfoils are compared to appreciate the difference in the results. The aerodynamic efficiency computed for all the three optimization strategies with the HF model is presented in Fig. 21(a), which shows that the HF and MF results present similar trend in terms of aerodynamic efficiency. Both results exhibit an overall efficiency which is higher than the one obtained by the LF optimization; this is explained in Fig. 21(b) by the behavior of the wave drag coefficient C_{D_W}, which is computed as the integral of the momentum defect over the streamtubes in the region outside the boundary layer.[57] The LF airfoil suffers from a larger drag penalty for higher values of the angle of attack. In fact, the effect of compressibility is greater at higher angle of attack with respect to the HF result. Addittionally, the increase in the drag coefficient due to compressibility appears at a lower value of the angle of attack. The result of the HF optimization does not suffer from a harsh drop off after the maximum of the aerodynamic efficiency is reached, thereby postponing the drag rise due to compressibility effects. In this respect, the MF result represents a trade-off solution between the two results.

With regard to computational cost, the number of evaluations of the solvers is presented in Table 9. The comparison proves that the computational effort of the HF method is reduced by 60% with the MF strategy. Also, the MF strategy employs one third of the HF evaluations required by the full HF optimization. This proves the main benefit of the

Table 9. Comparison of computational cost of different robust optimization strategies at $r = 0.8$: cost is computed considering 1 cost unit for each HF evaluation and 0.1 cost unit for each LF evaluation.

	LF	HF	MF
LF evaluations	32600	-	29166
HF evaluations	-	33475	10324
Cost	3260	33475	13241

proposed MF strategy, which generates solutions very close to the HF ones, but with a strong reduction of the computational cost. The MF strategy is thus capable of indicating regions of improvement in the design space, whereas a detailed analysis of the optimal solutions is left to higher fidelity methods and/or wind tunnel testing.

2. *Analysis of optimal airfoils*

To understand the validity of the robust approach in the outboard case as well, the HF results are discussed in more detail. With regard to the Pareto front airfoils presented in Fig. 20, it appears that the relationship between the optimal mean airfoils and the optimal variance airfoils found in the inboard section case, still holds. The optimal mean airfoils tend to be those with a mild curvature at the leading edge and more rear loaded. The

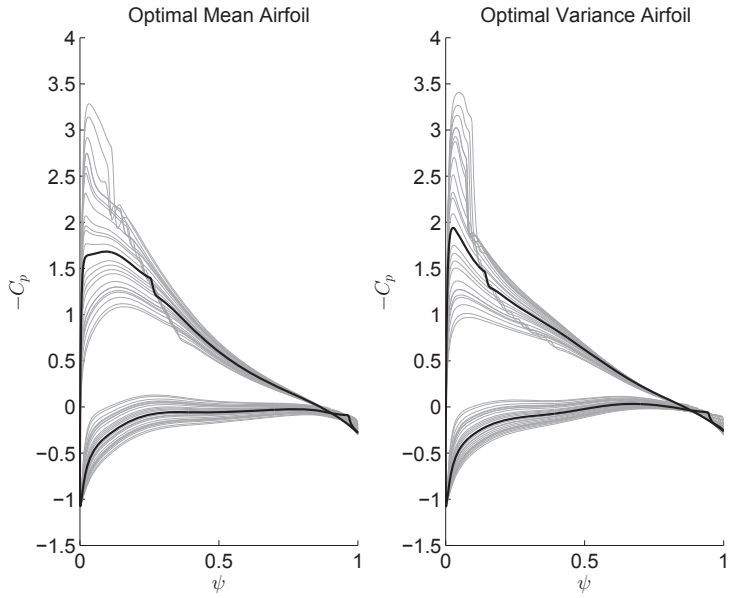

Figure 22. Comparison of the pressure coefficient of the optimal airfoils (HF) at $r = 0.8$: a thick black line is employed for the nominal condition and thin grey lines for the remaining samples.

optimal variance airfoils present a higher curvature at the leading edge. Indeed, the analysis of the pressure coefficient of the two airfoils, presented in Fig. 22, shows that the optimizer generates an optimal mean airfoil with an almost flat region of pressure coefficient behind the leading edge and reduces the number of operating conditions in the considered range for which a weak shock wave occurs. The optimal variance instead counteracts the growth of the lift coefficient resulting from the increase in the angle of attack, by producing a shock wave behind the peak close to the leading edge in a larger range of operating conditions. This balance results in a lower variance, at the expense of lower aerodynamic efficiency.

VI. Conclusions

The robust optimization technique based on Polynomial Chaos expansion and a genetic algorithm is capable of dealing with the range of operating conditions encountered when tackling the uncertainty-based design case presented. When considering uncertainties in the operating conditions, different flow regimes could be encountered in the domain defined by the stochastic variables, which require specific physical models and numerical solvers. The multi-fidelity strategy proposed in the work deals with two different models of the aerodynamics which have different accuracy and computational cost. In particular, a rapid estimation is obtained by means of a panel/integral boundary layer method for the stochastic sample associated with subsonic flow conditions, while a coupled Euler equations/integral boundary layer solver is employed for those operating conditions in the stochastic variables domain that exhibit important compressible effects. A switching logic is used for each design to determine which samples should be computed by the rapid low-fidelity or by the high-fidelity codes. The method proved effective in finding airfoils that improve the aerodynamic efficiency, by postponing the boundary layer transition to turbulence in the subsonic case, and by reducing the drag due to compressibility effects in the low transonic case, in the range of considered operating conditions. The multi-fidelity strategy reduces the computational cost by 60% with respect to the high-fidelity strategy, and results in Pareto airfoils consistent to the high-fidelity results. Thus, the proposed method is well-suited to indicate regions of improvement in the design space, which can be later analysed in detail by means of a high-fidelity model. In addition, the multi-fidelity strategy could be easily applied to other models at one's disposal, and it could be extended to other flowfield characteristics and physical models. Furthermore, the robust optimization proved to be a reliable and effective design tool when compared with two deterministic approaches.

The employment of robust optimization is thus expected to be of great interest in the application of helicopter rotor airfoils, owing to the fact that even the airfoils with higher mean values achieve lower values of the variance of the aerodynamic efficiency with respect

to variations of the angle of attack. The reduction of the variance could lead for instance to a reduction of the required rotor shaft torque in variable operating conditions. A complete optimization of the airfoil for its application on a helicopter rotor will require to include the analysis of the forward flight conditions together with the hover. The extension of the presented approach to forward flight will affect only the characterization of the uncertainty intervals of the variables and the choices associated with them, i.e. the selection of the control points and of the most appropriate physical models for each flow condition. However, the proposed multi-fidelity physics-based strategy will be still applicable as is also to this case. Finally, the paper provides a first set of results in the uncertainty-based aerodynamic optimization of rotor blade airfoils in hover.

Acknowledgments

The authors from Politecnico di Milano wish to acknowledge the financial support of the Politecnico di Milano to this project through the FARB (Fondo di Ateneo per la Ricerca di Base).

References

[1]Jameson, A., "Aerodynamic shape optimization using the adjoint method," *Lectures at the Von Karman Institute*, 2003.

[2]Hicks, R. M. and Henne, P. A., "Wing Design by Numerical Optimization," *Journal of Aircraft*, Vol. 15, No. 7, 1978, pp. 407–412.

[3]Jameson, A., "Optimum aerodynamic design using CFD and control theory," *12th Computational Fluid Dynamics Conference, San Diego, CA*, 1995.

[4]Elliott, J. and Peraire, J., "Practical Three-Dimensional Aerodynamic Design and Optimization Using Unstructured Meshes," *AIAA Journal*, Vol. 35, No. 9, 1997, pp. 1479–1485.

[5]Jameson, A., Alonso, J., Reuther, J., and Matrinelli, L., "Aerodynamic Shape Optimization Techniques Based On Control Theory," 1998.

[6]Mäkinen, R. A. E., Periaux, J., and Toivanen, J., "Shape design optimization in 2D aerodynamics using Genetic Algorithms on parallel computers," *Parallel Computational Fluid Dynamics*, Elsevier Science, 1995, pp. 395–402.

[7]Morris, A. M., Allen, C. B., and Rendall, T. C. S., "Development of generic CFD-based aerodynamic optimisation tools for helicopter rotor blades," *25th AIAA Applied Aerodynamics Conference, AIAA, Miami, FL*, June 2007.

[8]Tatossian, C. A., Nadarajah, S. K., and Castonguay, P., "Aerodynamic shape optimization of hovering rotor blades using a Non-Linear Frequency Domain approach," *Computers and Fluids*, Vol. 51, No. 1, 2001, pp. 1–15.

[9]Collins, K., Sankar, L., and Mavris, D., "Application of Low- and High-Fidelity Simulation Tools to

Helicopter Rotor Blade Optimization," *Journal of the American Helicopter Society*, Vol. 58, No. 4, October 2013, pp. 1–10.

[10]Allen, C. B. and Rendall, T. C. S., "Computational-Fluid-Dynamics-Based Twist Optimization of Hovering Rotors," *Journal of Aircraft*, Vol. 47, No. 6, 2010, pp. 2075–2085.

[11]Allen, C. and Rendall, T., "CFD-based optimization of hovering rotors using radial basis functions for shape parameterization and mesh deformation," *Optimization and Engineering*, Vol. 14, No. 1, 2013, pp. 97–118.

[12]Le Pape, A. and Baumier, P., "Numerical optimization of helicopter rotor aerodynamic performance in hover," *Aerospace Science and Technology*, Vol. 9, No. 3, April 2005, pp. 191–201.

[13]Beyer, H.-G. and Sendhoff, B., "Robust optimization - A comprehensive survey," *Computer Methods in Applied Mechanics and Engineering*, Vol. 196, No. 33-34, July 2007, pp. 3190–3218.

[14]Schuëller, G. I. and Jensen, H. A., "Computational methods in optimization considering uncertainties An overview," *Computer Methods in Applied Mechanics and Engineering*, Vol. 198, No. 1, Nov. 2008, pp. 2–13.

[15]Yao, W., Chen, X., Luo, W., van Tooren, M., and Guo, J., "Review of uncertainty-based multidisciplinary design optimization methods for aerospace vehicles," *Progress in Aerospace Sciences*, Vol. 47, No. 6, Aug. 2011, pp. 450–479.

[16]Helton, J. C., Johnson, J. D., and Oberkampf, W. L., "An exploration of alternative approaches to the representation of uncertainty in model predictions," *Reliability Engineering & System Safety*, Vol. 85, No. 1–3, 2004, pp. 39–71.

[17]Rumpfkeil, M. P., "Optimizations Under Uncertainty Using Gradients, Hessians, and Surrogate Models," *AIAA Journal*, Vol. 51, No. 2, 2013, pp. 444–451.

[18]Padulo, M., Campobasso, M. S., and Guenov, M. D., "Novel Uncertainty Propagation Method for Robust Aerodynamic Design," *AIAA Journal*, Vol. 49, No. 3, March 2011, pp. 530–543.

[19]Dodson, M. and Parks, G. T., "Robust Aerodynamic Design Optimization Using Polynomial Chaos," *Journal of Aircraft*, Vol. 46, No. 2, 2009, pp. 635–646.

[20]Huyse, L., Padula, S. L., Lewis, R. M., and Li, W., "Probabilistic Approach to Free-Form Airfoil Shape Optimization Under Uncertainty," *AIAA Journal*, Vol. 40, No. 9, 2002, pp. 1764–1772.

[21]Lee, D. S., Periaux, J., Onate, E., Gonzalez, L. F., and Qin, N., "Active Transonic Aerofoil Design Optimization Using Robust Multiobjective Evolutionary Algorithms," *Journal of Aircraft*, Vol. 48, No. 3, 2011, pp. 1084–1094.

[22]Jakeman, J., Eldred, M., and Xiu, D., "Numerical approach for quantification of epistemic uncertainty," *Journal of Computational Physics*, Vol. 229, No. 12, June 2010, pp. 4648–4663.

[23]Zhang, Y., Hosder, S., Leifsson, L., and Koziel, S., "Robust airfoil optimization under inherent and model-form uncertainties using stochastic expansions," *50th AIAA Aerospace Sciences Meeting including the New Horizons Forum and Aerospace Exposition, AIAA, Nashville, TN*, January 2012.

[24]Spalart, P. and Allmaras, S., "A one-equation turbulence model for aerodynamic flows," *30th Aerospace Sciences Meeting and Exhibit, AIAA, Reno, NV*, January 1992.

[25]Le Maître, O. P. and Knio, O. M., *Spectral methods for uncertainty quantification. With Applications to Computational Fluid Dynamics.*, Springer, 2010.

[26]Drela, M., "XFOIL: An Analysis and Design System for Low Reynolds Number Airfoils." *Conference on Low Reynolds Number Airfoil Aerodynamics, University of Notre Dame*, Vol. 54, 1989, pp. 1–12.

[27]Jones, B. R., Crossley, W. A., and Lyrintzis, A. S., "Aerodynamic and aeroacoustic optimization of rotorcraft airfoils via a parallel genetic algorithm," *Journal of Aircraft*, Vol. 37, No. 6, 2000, pp. 1088–1096.

[28]Vu, N. A., Lee, J. W., and Shu, J. I., "Aerodynamic design optimization of helicopter rotor blades including airfoil shape for hover performance," *Chinese Journal of Aeronautics*, Vol. 26, No. 1, 2013, pp. 1–8.

[29]Massaro, A. and Benini, E., "Multi-Objective Optimization of Helicopter Airfoils Using Surrogate-Assisted Memetic Algorithms," *Journal of Aircraft*, Vol. 49, No. 2, March 2012, pp. 375–383.

[30]Choi, S., Alonso, J. J., and Kroo, I. M., "Two-Level Multifidelity Design Optimization Studies for Supersonic Jets," *Journal of Aircraft*, Vol. 46, No. 3, 2009, pp. 776–790.

[31]Robinson, T. D., Willcox, K. E., S., E. M., and Haimes, R., "Multifidelity Optimization for Variable-Complexity Design," *11th AIAA/ISSMO Multidisciplinary Analysis and Optimization Conference, AIAA, Portsmouth, VA*, September 2006.

[32]Leusink, D., Alfano, D., and Cinnella, P., "Multi-fidelity optimization strategy for the industrial aerodynamic design of helicopter rotor blades," *Aerospace Science and Technology*, Vol. 42, No. 0, 2015, pp. 136–147.

[33]Yamazaki, W., "Efficient Robust Design Optimization by Variable Fidelity Kriging Model," *53rd AIAA/ASME/ASCE/AHS/ASC Structures, Structural Dynamics and Materials Conference, AIAA, Honolulu, HI*, April 2012.

[34]Yamazaki, W. and Mavriplis, D. J., "Derivative-Enhanced Variable Fidelity Surrogate Modeling for Aerodynamic Functions," *AIAA Journal*, Vol. 51, No. 1, 2103, pp. 126–137.

[35]Ng, L. W.-T. and Eldred, M., "Multifidelity Uncertainty Quantification Using Non-Intrusive Polynomial Chaos and Stochastic Collocation," *53rd AIAA/ASME/ASCE/AHS/ASC Structures, Structural Dynamics and Materials ConferenceAIAA, Honolulu, HI*, April 2012.

[36]Leifsson, L. and Koziel, S., "Multi-fidelity design optimization of transonic airfoils using physics-based surrogate modeling and shape-preserving response prediction," *Journal of Computational Science*, Vol. 1, No. 2, pp. 98–106.

[37]Johnson, W., *Rotorcraft Aeromechanics*, Cambridge University Press, New York, 2013.

[38]Bousman, W. G., "Airfoil Design and Rotorcraft Performance." *American Helicopter Society 58th Annual Forum, Montreal, Canada*, 2002.

[39]van der Wall, B. G., *2nd HHC Aeroacoustic Rotor Test (HART II) - Part I: Test Documentation.*, Braunschweig, Germany, 2003.

[40]Leishman, J., *Principles of helicopter aerodynamics. 2nd edition*, Cambridge University Press, 2006.

[41]Siva, C., Murugan, M. S., and Ganguli, R., "Uncertainty Quantification in Helicopter Performance Using Monte Carlo Simulations," *Journal of Aircraft*, Vol. 48, No. 5, Sept. 2011, pp. 1503–1511.

[42]Pediroda, V., Poloni, C., and Clarich, A., "A Fast and Robust Adaptive Methodology for Airfoil Design Under Uncertainties based on Game Theory and Self-Organising-Map Theory," *44th AIAA Aerospace Sciences Meeting and Exhibit, AIAA, Reno, NV*, January 2006.

[43]Simon, F., Guillen, P., Sagaut, P., and Lucor, D., "A gPC-based approach to uncertain transonic aerodynamics," *Computer Methods in Applied Mechanics and Engineering*, Vol. 199, 2010, pp. 1091–1099.

[44]Abdallah, I., Natarajan, A., and Srensen, J., "Impact of uncertainty in airfoil characteristics on wind turbine extreme loads," *Renewable Energy*, Vol. 75, Jan. 2015, pp. 283–300.

[45]Shapiro, A. H., *The Dynamics and Thermodynamics of Compressible Fluid Flow*, Vol. I, The Ronald Press Company, 1953.

[46]Giles, M. B. and Drela, M., "Two-dimensional transonic aerodynamic design method," *AIAA Journal*, Vol. 25, No. 9, 1987, pp. 1199–1206.

[47]Drela, M., "Implicit Implementation of the Full e^n Transition Criterion," *21st Applied Aerodynamics Conference, Orlando, FL*, June 2003.

[48]Giles, M. B. and Drela, M., "Viscous-inviscid Analysis of Transonic and Low Reynolds Number Airfoils," *AIAA Journal*, Vol. 25, No. 10, 1987, pp. 1347–1355.

[49]Kulfan, B. M. and Bussoletti, J. E., ""Fundamental" Parametric Geometry Representations for Aircraft Component Shapes," *11th AIAA/ISSMO Multidisciplinary Analysis and Optimization Conference, Portsmouth, VA*, September 2006.

[50]Srinivas, N. and Deb, K., "Multiobjective function optimization using nondominated sorting genetic algorithms," *Evolutionary Computation*, Vol. 2, No. 3, 1994, pp. 221–248.

[51]Congedo, P. M., Corre, C., and Martinez, J.-M., "Shape optimization of an airfoil in a BZT flow with multiple-source uncertainties," *Computer Methods in Applied Mechanics and Engineering*, Vol. 200, No. 1–4, 2011, pp. 216–232.

[52]Xiu, D. and Karniadakis, G. E., "The Wiener–Askey Polynomial Chaos for Stochastic Differential Equations," *SIAM Journal on Scientific Computing*, Vol. 24, No. 2, Jan. 2002, pp. 619–644.

[53]Jin, Y., Olhofer, M., and Sendhoff, B., "A Framework for Evolutionary Optimization With Approximate Fitness Functions," *IEEE Transactions on Evolutionary Computation*, Vol. 6, 2002, pp. 481–494.

[54]Marti, L. and García, J., "An approach to stopping criteria for multi-objective optimization evolutionary algorithms: the MGBM criterion," *Evolutionary Computation*, 2009, pp. 1263–1270.

[55]Goel, T. and Stander, N., "A study on the convergence of multiobjective evolutionary algorithms," *13th AIAA/ISSMO Multidisciplinary Analysis Optimization Conference, Forth Worth, TX*, September 2010.

[56]Shen, H., McBean, E., and Wang, Y., "Sensor Placement Under Nodal Demand Uncertainty for Water Distribution Systems," *Securing Water and Wastewater Systems*, edited by R. M. Clark and S. Hakim, Vol. 2 of *Protecting Critical Infrastructure*, Springer International Publishing, 2014, pp. 123–133.

[57]Drela, M., *A User's Guide to MSES 3.05*, MIT Department of Aeronautics and Astronautics, 2007.